Ocean Sci. Discuss., 11, 47–122, 2014
www.ocean-sci-discuss.net/11/47/2014/
doi:10.5194/osd-11-47-2014

Ocean Science
Discussions
Open Access

Possible signals of poleward surface ocean heat transport, of Arctic basal ice melt, and of the twentieth century solar maximum in the 1904–2012 Isle of Man daily timeseries

J. B. Matthews[1] **and J. B. R. Matthews**[1,2]

[1]Tennis Road, Douglas, Isle of Man, British Isles
[2]School of Earth and Ocean Sciences, University of Victoria, Victoria, BC, Canada

Received: 23 September 2013 – Accepted: 12 December 2013 – Published: 3 January 2014

Correspondence to: J. B. Matthews (drs-matthews@manx.net)

Published by Copernicus Publications on behalf of the European Geosciences Union.

Abstract

This is the second of two papers on observational timeseries of top of ocean heat capture. The first reports hourly and daily meridional central tropical Pacific top 3 m timeseries showing high Southern Hemisphere evaporation (2.67 m yr^{-1}) and Northern Hemisphere trapped heat (12 MJ m^{-2} day^{-1}). We suggested that wind drift/geostrophic stratified gyre circulation transported warm water to the Arctic and led to three phases of Arctic basal ice melt and fluxes of brackish nutrient-rich waters to north Atlantic on centennial timescales.

Here we examine daily top metre 1904–2012 timeseries at Isle of Man west coast ~ 54° N for evidence of tropical and polar surface waters. We compare these to Central England (CET) daily land-air temperatures and to Arctic floating ice heat content and extent.

We find three phases of ocean surface heating consistent with basal icemelt buffering greenhouse gas warming until a regime shift post-1986 led to the modern surface temperature rise of ~ 1 °C in 20 yr. Three phases were: warming +0.018 °C yr^{-1} from 1904–1939, slight cooling −0.002 °C yr^{-1} 1940–86 and strong warming +0.037 °C yr^{-1} 1986–2012. For the same periods CET land-air showed: warming +0.015 °C yr^{-1}, slight cooling −0.004 °C yr^{-1}, about half SST warming at +0.018 °C yr^{-1}. The mid-century cooling and a 1959/1963 hot/cold event is consistent with sunspot/solar radiation maximum 1923–2008 leading to record volumes of Arctic ice meltwater and runoff that peaked in 1962/3 British Isles extreme cold winter.

The warming Arctic resulted in wind regime and surface water regime shifts post 1986. This coincides with the onset of rapid Arctic annual ice melt. Continued heat imbalance is likely to lead to tidewater glacier basal icemelt and future sealevel rise after remaining relatively stable over 4000 yr. Our work needs confirmation by further fieldwork concentrating on the dynamics and thermodynamics of ocean top 3 m that controls the 93 % anthropogenic global warming in the oceans. This may be done most

cost-effectively through focussed multidisciplinary scientific research adaptively managed and funded.

1 Introduction

This is the second of two papers presenting unique experimental evidence of the dynamic and thermodynamic processes in the upper 2 m ocean. Anthropogenic global warming (AGW) or heat imbalance for the past 250 yr can be explained from models of volcanism and the log of top-of-the atmosphere CO_2 concentration without reference to solar irradiance variations (Rohde et al., 2013). This was determined from centennial daily land-air timeseries. Heat and mass cannot pass the land-air boundary. They behave differently in the surface boundary layer. Turbulent buoyancy dynamics are calculated from 10 m winds and 2 m meteorological data (Taylor, 1931). Buoyant fluxes carry heat and mass aloft to the top of the atmosphere. Thus, volcanism and greenhouse gas concentration determine infrared solar irradiance heat imbalance or AGW at the top of the atmosphere.

Land-air buoyancy parameterisation does not apply at the sea-air boundary heated from the top (Matthews and Matthews, 2013). Heat and mass pass through the buoyant boundary layer. Seawater buoyancy depends on density that is a function of both temperature and salinity. Salinity introduces a negative term in the buoyancy equation. Evaporation from surface heating produces stratification and circulation dependent on seawater density (Turner, 1998). We found bulk parameterisation based on land-air buoyancy do not apply at the tropical equatorial surface ocean boundary (Matthews and Matthews, 2013). However, more AGW-heat is in the top 2 m than in the entire atmosphere above. Almost all solar irradiance is captured in this layer (Soloviev and Lukas, 2006). Oceans have 93 % of observed AGW (Levitus et al., 2012). It is therefore important to use the appropriate thermodynamic characterisation of sea evaporation and ocean heat capture. Hourly and daily timeseries are required although these are not usually available at sea.

Evaporation depends on sea surface temperature and surface buoyancy. It is highest at the equator. It derives from the vapour pressure difference between air and water. Sea surface temperature, not air temperature, determines vapour pressure and hence evaporation. Saturation equilibrium vapour pressure increases by 7 % $^{\circ}C^{-1}$, (Clausius–Clapeyron relation), while precipitation increases at 2–3 % $^{\circ}C^{-1}$. It is an exponential function and is most effective at tropical temperatures > 20 °C. The Humboldt Current flows northwards at 15 °C at 40° S and then along the Atacama Desert. Evaporation shows only early morning dew and precipitation is extremely rare. The same water, 4.5 yr and 19 000 km later, is in mid-Pacific at 140° W at 28 °C and evaporated at the rate of 2.67 m m^{-2} yr^{-1} and sequestered heat of 6 MJ m^{-2} day^{-1} below 3 m (Matthews and Matthews, 2013). Buoyant water in the Northern Hemisphere tropics at mean temperatures ∼ 26 °C evaporated 1.67 m m^{-2} yr^{-1} and sequestered 12 MJ m^{-2} day^{-1}. No correlation with wind speed or humidity was found. Surface temperature correlated to nocturnal cooling just south of Hawaii.

Seawater density increases with increasing salinity, but decreases with increasing temperature (Rooth, 1982). Double diffusion results when warm salty water meets cold brackish water (Turner, 1998). Heat passes to colder water faster than salt. Denser salty water sinks. There is a surface salt gradient from the equator to the poles. A salt/heat (alpha/beta) boundary was found in the north Pacific and Atlantic at abrupt fronts at SST of ∼ 10 °C Carmack (2007). We found an abrupt front with surface temperature difference > 1 °C in 12 km at ∼ 11° N in the north Pacific (Matthews and Matthews, 2013). Fronts mark the loci of brine sinking in the alpha/beta ocean conveyor system (Carmack, 2007). Strong Lagrangian surface wind-drift/geostrophic currents run along the frontal boundaries in the top 2 m of the ocean, the jet streams of the ocean. The distribution of thermohaline stratified, low salinity, nutrient-rich surface waters was described as a downhill journey along pycnoclines from the stratified north Pacific, through 50 m-deep Bering Strait and the highly-stratified Arctic Ocean, to the North Atlantic (Carmack, 2007).

The equatorial Pacific has two surface circulation systems separated by equatorial upwelling and the eastbound Equatorial Undercurrent (EUC) at 50–150 m depths (Matthews and Matthews, 2013). Salinity > 36.4 ‰ and temperature > 28 °C had high evaporation (2.67 m m^{-2} yr^{-1}) but cooled only for a short-time after sunset for heat sequestration below 3 m of only 6 MJ m^{-2} day^{-1}. The NH tropics, with full temperature-driven thermohaline circulation at lower temperature and salinity, captured about double the ocean heat at 12 MJ m^{-2} day^{-1}. This supports the concept of polar amplification in the Northern Hemisphere. Meridional horizontal heat and mass transport was limited by wind-driven upwelling and thermohaline sinking in pairs of counter-rotating vertical meridional tropical cells (MTC). These were ∼ 300–100 km wide and ∼ 100 m deep, part of which were observed by Perez et al. (2010). Vertical transport was at 0.8–10 m day^{-1}. Meridional geostrophic transport is an order of magnitude smaller than zonal wind-driven/geostrophic transport. Surface water flowed down pycnoclines from the equator and from about 20° N and 17° S to downward brine sinking points about 5° N and 5° S. These were at the centre of westward-bound surface gyres.

A zonal system of eleven interconnected counter-rotating divergent/convergent Lagrangian surface wind-drift/geostrophic gyres link the Pacific/Arctic/Atlantic and world oceans (Ebbesmeyer and Scigliano, 2009). Ekman wind-driven near-surface currents are modified in the upper 2 m of ocean by Lagrangian logarithmic wind drift currents (e.g. Pugh, 1987). The gyres incorporate Lagrangian coherent water masses that have only recently received attention although reported as early as 1954 (Peacock and Haller, 2013; Lin et al., 2013; Williamson, 1956). We adopt the gyre nomenclature proposed by Ebbesmeyer and Scigliano (2009) because they refer specifically to surface Lagrangian wind-driven/geostrophic gyres (Matthews and Matthews, 2013: Fig. 1). The gyre system has been confirmed from daily data 1902–1997 in the North Pacific with the OSCURS numerical model tuned to very extensive experimental Lagrangian surface drifter studies and daily geostrophic and surface wind data (Ingraham, 1997; Dat et al., 1995; Ebbesmeyer and Scigliano, 2009; Ebbesmeyer et al., 2011). Surface wind drift coefficients were verified for passive plankton-carrying watermasses and

surface drifters, self-propelled drifters and those with appreciable sail areas that are enhanced by 30–50 %. All oceans have convergent surface gyres in garbage patches (e.g. Lavender-Law et al., 2010; Maximenko et al., 2012; van Sebille et al., 2012; Lumpkin and Johnson, 2013).

The gyres carry stratified ocean surface water from the tropics to the polar regions in a global circulation system Matthews and Matthews, (2013) suggested three phases of basal Arctic ice melt on a centennial timescale based on near-surface dynamics of the stratified system carrying Pacific and Atlantic water. Atlantic influx of warm saline waters across the Greenland-Scotland ridge is estimated to be 8.5 Sv (1 Sv = 10^6 m^3 s^{-1}) (Beszczynska-Möller et al., 2011). Pacific influx through the constricted 50 m Bering Strait is an order of magnitude smaller. It is therefore our aim to look at the larger north Atlantic surface data for evidence of warming and icemelt.

Surface drifters showed that global surface counter-rotating gyre system carries almost all polar water eastbound to the European north Atlantic coast north of 50° N (Ebbesmeyer et al., 2011). The alpha/beta boundary between subpolar and subtropical was described as a wall. Similar experimental data in the north Pacific shows the landfall place varies seasonally and on a 20–30 yr cycle between 45–60° N with a mean at ∼ 54.4° N (Ingraham et al., 1998). We argue that Columbus and Viking surface drift gyres carry sub-tropical and sub-polar buoyant surface water to mean landfall on the western Irish coast at ∼ 54° N. Water from these subtropical and subarctic sources reach Port Erin mainly across the Malin ∼ 65 m sill and vary seasonally

The western Irish Sea is a classic 100 m-deep flooded V-shaped glacial valley fjord inlet though it has not been mentioned as a fjord in previous work (Fig. 1a and b). However, Herdman (1893) established Port Erin Marine Biological Station (PEMBS) because the Isle of Man had north Atlantic waters and species such as starfish not found at the first station at Menai, Anglesey in the eastern Irish Sea (Forbes, 1841). Herdman's (1920) depth profile through Port Erin clearly shows the contrast between the deep-V of the western fjord and the shallow eastern Irish Sea (Fig. 1b). There are similar fjords on the northwest Pacific coast with similar sills such as the 69 m Glacier Bay

and 62 m Muir Inlet sills at 58–59° N (Matthews and Quinlan, 1975; Matthews, 1981a). Semi-diurnal tidal flows over the sill continually cycle Pacific and fjord water across the sill. When density above the sill was greater outside than inside, seawater on a flood tide sank into the basin while less dense surface water left on the next ebb. During the November–April winter season of minimum freshwater input, Glacier Bay winter shelf waters were homogenous at 3 °C and salinity 33 ‰ (Matthews, 1981a). UK shelf waters are vertically homogenous in winter (Brown et al., 2003; Hydes et al., 2007). We suggest the Malin sill operates in similar way in the western Irish Sea fjord inlet to bring water to Port Erin. Surface water derives from residual semi-diurnal tidal and wind-drift currents on prevailing SW winds with occasional reversals from sustained wind shifts.

Arctic surface water produces brine from freezing in water of salinity 0 ‰ to 24.7 ‰. Like freshwater, it freezes after cooling to its temperature of maximum density at 4 °C to −1.7 °C without further vertical mixing (Matthews and Matthews, 2013). Arbitrary values of 35.2 ‰ and 34.8 ‰ are used to distinguish Pacific and North Atlantic warm water from Arctic surface water (Aagaard and Carmack, 1989; Wijffels et al., 1992; Dickson et al., 2007; Beszczynska-Möller et al., 2011). We use the methods of Dickson et al. (1988) in tracing salinity anomalies by looking for high anomalies (i.e. near Atlantic Gulf Stream water at ∼ 35.1 ‰) and low anomalies (below Port Erin long-term average 34.0 ‰) (Allen et al., 1998).

Kinsman (1956) pointed out the common statistical fallacy that correlates cause and effect. For example, Sharples et al. (2006) report correlations with observed SST of 0.3 to the onset of spring stratification, and 0.8 to modelled SST. The model was forced only by weather and radiation. Both are considered weak correlations and do not demonstrate causality (Kinsman, 1956). Conclusions arose from using inappropriate land-air parameterisations on SST data as reported (Matthews and Matthews, 2012).

Long timeseries are rare in geophysical sciences and therefore prone to the improper use of statistics (Kinsman, 1957). Kinsman wrote that there are generally data gaps or only short sequences so the temptation to fill gaps according to some unproven hypothesis is great. He noted a related problem was the inherent hazard in filling gaps

in data taken for other purposes. Results are often at variance with the underlying physics. Furthermore, he states: “The worst of all practices, however, is the artifice of adjusting the data to improve the correlation”.

We confirmed the misuse of statistics without experimental verification in the central tropical Pacific experiment (Matthews, 2012; Matthews and Matthews, 2012). Temperatures from three types of bucket were found equal to each other and contemporaneous CTD, satellite and buoy data. Data alterations applied for evaporative cooling of bucket samples were not justified because the short sample time (< 1 min) was insufficient for skin evaporative cooling to reach the thermo sensor. An absurd correction had been applied for engine room warming of temperatures of engine intake seawater, often taken at unknown depths, that flowed through pipes at 1.5 m s^{-1} and measured ∼ 1.5 m from the inlet port. We argue that even with 50 °C engine room temperatures, measurable water heating is unlikely considering the 3000x difference in heat capacities and the time available (∼ 1 s) to the sensor. Indeed, if such heat transfer were experimentally viable, we would use our domestic water circulation baseboard heaters for summer air conditioner cooling as well as for winter heating. Another wrong assumption was that seawater has the uniform temperature over the upper 10 m. Soloviev and Lukas (2006), and Soviet Russian researchers decades earlier showed there were near-surface gradients cooling with depth in all the world oceans. Central mid-equatorial Pacific temperature differences over 0–3 m depth averaged a fall of –0.4 °C and could be as high as −1 °C (Matthews and Matthews, 2012, 2013). Indeed, we suggested these experimentally unverified alterations be removed from datasets. Otherwise, important regime shifts were removed from the 20th century record. The misuse of statistics and disregard of basic physics continues to this day in Atmospheric Physics (Aberson, 2009). Moreover, ocean heat content datasets that incorporate experimentally unverified SST alterations for the mid C20th to the 1990s are unlikely to be secure for this period (e.g. Levitus et al., 2012). We therefore restrict our study of the top 3 m surface physics to long-term daily observational datasets taken to oceanographic standards.

The aim of this paper is to show three phases of ocean warming and its connection to anthropogenic global warming and basal Arctic icemelt. We first review historical data. Then we examine 1903–2012 daily sea surface temperatures from Port Erin for trends compared to Central England (CET) land-air temperature. We relate the 1959/1963 warm/cold event to a major sunspot irradiance peak September 1957–January 1958 and subsequently to enhanced Arctic icemelt. We examine the extreme winter 1962/3 cold SST data in relation to other extreme winters. We then examine TS density cycles from 1982 to 2007 that demonstrate a post-1986 warming trend. We look for change in wind regimes from 1960 to the early 2000s. We then compare our north Atlantic-heating cycles to those in the Arctic ice records from 1979 to show a post-1986 heating. Finally, we discuss how this relates to the hypothesis of polar amplification due to the stratified Pacific/Arctic/Atlantic near-surface heat and mass transport system and ocean AGW.

1.1 Historical perspective

The British Isles were part of the European landmass until the last great Holocene glacial retreat and flooding over last 250 kyr (Cunliffe, 1997; Turney and Brown, 2007). The last glacial ice maximum advance 20 kyr BP covered the Isle of Man (Fig. 1a), (Rasmussen et al., 2006; Cook, 2013). At the end of the last ice age, Lake Agassiz flowed through Canadian archipelago and into north Atlantic (Murton et al., 2010). Bond et al. (1997) showed ice rafted debris in the European Atlantic. The last great flood from the melting of the Laurentide ice sheet was about ∼ 7900 yr BP (Kennett et al., 2008). This flooded the Irish Sea western fjord over the North Channel ∼ 65 m sill and ∼ 90 m deep Celtic Sea sill (Fig. 1a). At the same time the 50 m deep Bering Strait opened the Pacific surface connection to the Arctic Ocean. Up to this time the Pacific Ocean circulation was completely separate from the Atlantic-Arctic Oceans. Indeed, we showed that Northern Hemisphere surface waters are landlocked in the Indian Ocean, almost land-locked in the Pacific with the Arctic and Atlantic freely connected (Matthews and Matthews, 2013). The southern ocean connects all oceans but equatorial divergence separates surface circulation. The Arctic freshwater flux into the

North Atlantic has been a major feature of North Atlantic circulation for at least the last 4000 yr (Mernild et al., 2012). Gebbie (2012) argues that meltwater reached abyssal depths over a period of ∼ 1750 yr with the Pacific lagging Atlantic deep waters by ∼ 4000 yr.

For the past 4000 yr sea level has been constant suggesting relatively stable ice sheets until AGW began 250 yr with the industrial revolution (Matthews and Matthews, 2013; Post et al., 2011). The UK has been continuously occupied and witness to these changes. The British Isles were conveniently situated on global seafaring network of interconnected oceans, seas and rivers from the beginning of the Bronze Age industrial revolution (Cunliffe, 1997, 2008). The world's first map, a Babylonian clay tablet in the British Museum shows the earth as land surrounded by the circular southern ocean (Jacobs, 2004). Ancient mariners would not be afraid to drop off the flat earth as were medieval explorers. Pleistocene cave art is firmly dated to 12.8 kyr BP at Creswell Crags that was first occupied 30 kyr BP in Central England (marked Pc in Fig. 1a) (Pike et al., 2005). Kendrick's Cave, Great Orme, North Wales (marked Po, Fig. 1a) was also occupied at the same time (Cook, 2013). Copper was smelted on Great Orme for 6000 yr during the Bronze Age (Cunliffe, 2008). The remains of a copper mine can be seen at the entrance to Port Erin bay at the cliff bottom opposite the former PEMBS marine station (Fig. 1c). Cornwall, England was a major source of rare tin traded from the typical Phoenician island port connected to the mainland by a causeway at St Michaels Mount (Pme on Fig. 1c). Greek Dionysius of Syracuse in 397 BC sacked Motya in western Sicily and it was never reoccupied (Matthews, 1963; Isserlin and Taylor, 1974). It has the best-preserved island-causeway that was thought to be founded ∼ 2800–2900 BP. However, recent research on shells under the tufa block causeway showed it was laid ∼ 3600 yr BP (Basso et al., 2008). High-wheeled Sicilian carts still cross the submerged causeway as they did in ancient times. Thus, sealevel has been relatively unchanged for at least the last ∼ 4000 yr. We suggest depletion of Arctic floating ice will increase basal melting of tidewater glaciers (Matthews and Matthews, 2013). Future sealevels are likely to rise substantially.

Though long-term solar irradiance variations do not influence the last 250 yr AGW, decadal variations do influence ocean cycles. Many climate index timeseries such as the El Niño/La Niña index (Nino3.4), the Southern Oscillation Index (SOI), the Pacific Decadal Oscillation (PDO), the North Pacific Index (NPI), the North Atlantic Oscillation (NAO), the Atlantic Multidecadal Oscillation (AMO) and the South and North Pacific PC1 indices (SPC1, NPC1) are based on solar resonant or phase-locked harmonics (Douglass and Knox, 2012). The correlation coefficient between the equatorial sea surface temperature (SST) and pressure anomalies was reported to be greater than 0.8 (Swanson and Tsonis, 2009). Challenger datasets from 1872–76, about 100 yr after the beginning of the industrial revolution, suggest mean global ocean temperatures rose over 135 yr by 0.59±0.12 °C at the surface, by 0.39±0.18 °C below 366 m (200 fathoms) and by 0.12 ± 0.07 °C at 914 m (500 fathoms) (Roemmich et al., 2012). This suggests 2/3 of surface heat reached 366 m after about 135 yr. We found 2/3 of surface heat was trapped below 3 m in MTCs to 100 m in the central north Pacific (Matthews and Matthews, 2013). Thus, the surface ocean warming is on a centennial timescale while the deep ocean is millennial as noted by Rooth (1982).

1.2 Modern British atmospheric and ocean science

Admiral Fitzroy founder of the UK Met Office established global observations from ships, lighthouses, and weatherships (Mellersh, 1974). Ocean weatherships were valuable resources for trans-ocean voyages and extended into the 1970s to provide bulletins to aircraft (Downes, 1977). The last ocean weathership "M"/"Mike" ceased operation at the end of 2009. Subsequently satellites and moored and drifting buoys replaced weatherships as inter-continental aircraft replaced ocean liners and very large container ships and tankers replaced general cargo vessels. Much of the detail of ocean processes on thermohaline, tidal and wind-driven circulation developed in the Irish Sea was not carried forward into global ocean near-surface studies.

1.2.1 Western Irish Sea surface currents

The western Irish Sea surface water is subject to semi-diurnal tidal flushing and wind-driven surface drift currents. Net south-north throughflow flow is sufficient to replace the Irish Sea water in one year (Knight and Howarth, 1999). A substantial fraction of annual flushing can take place in during one sustained storm. We suggest the upper few metres are carried on Lagrangian surface drift currents at far higher speeds than Eulerian currents as observed by Williamson (1956). The deep Western Irish is able to maintain stratification while the eastern Irish Sea is a well-mixed shallow coastal sea fed by coastal plain estuaries (Fig. 1b). Simpson and Hunter (1974) parameterised the stratification/shear frontal system between the stratified and well-mixed systems.

A tidal model of the M_2 tide showed the western Irish Sea gyre and partial tidal current amphidrome in the co-range and current-amplitude-isolines (Mungall and Matthews, 1978). A film of the model output clearly showed flood tides sweeping up St George's Channel into Liverpool bay. The southbound North Channel flood met the St George's flood southwest of the Isle of Man in the partial amphidrome. The tidal current null area or current amphidrome is a roughly triangular area between Dublin, Carlingford, and Calf Island, off the southwest tip of the Isle of Man at the confluence of tides from north and south (Pugh, 1981). Tidal elevations rise and fall but has permanently slack water with no tidal surface currents (Fig. 1c). The film and model clearly showed the Coriolis effect whereby the tidal range is higher on the outside of the cyclonic flood circulation and anticylconic ebb. Therefore, both Strangford and Liverpool have higher tidal ranges than the Isle of Man.

Tidal streams 3 h before and after HW are shown and range from 0.7–1.2 $m s^{-1}$ on the ~ 7 h flood and ~ 0.8–1.4 $m s^{-1}$ on the ~ 5 h ebb (Fig. 1c). Williamson (1957) reported plankton-carrying watermasses travelling 145–320 km from North Channel to the Scottish west coast over 2 days of strong SW winds. Eulerian residual calculations suggested travel of only ~ 800 $m day^{-1}$. The shorter distance travelled was into a fjord cul de sac. The longer distance is consistent with wind-drift currents ~ 3 % of

windspeed as verified for the OSCURS wind-drift gyre model (Ingraham, 1997). More drifter studies are needed for better definition of drift coefficients, periods and sub-gyre variation over time.

Details on the seasonal cold dome stratified gyre over the cold-trapped winter water have come from models verified by observation (Simpson, 1971; Simpson and Hunter, 1974; Simpson et al., 1990; Hill et al., 1994; Horsburgh and Hill, 2003; Young et al., 2004; Verspecht et al., 2010; Olbert et al., 2011). Currents are $\sim 0.14\,\mathrm{m\,s^{-1}}$. The seasonal gyre has important ecological impacts (Horsburgh et al., 2000; Butler et al., 2010; Dabrowski et al., 2010). Models suggest seasonal warm brackish water accumulates in the upper gyre (Horsburgh and Hill, 2003).

The southern Celtic Sea gyre restricts surface Atlantic water penetration into the Irish Sea (Pugh, 1981; Brown et al., 2003; Hydes et al., 2004). The cyclonic gyre circulates water from Lands End and Bristol Channel to southwest Ireland into a complex shelf current that had a southbound cold current. The effect of the two cyclonic gyre systems (western Irish Sea, Celtic Sea) is to ensure surface waters at Port Erin are mainly from the North Channel on the cyclonic tidal system combined with net wind-drift currents (Knight and Howarth, 1999; Davies et al., 2002; Jones and Davies, 2003; Andreu-Burillo et al., 2007). Surface water travels along the Irish coast to the gyre boundary just to the south of the Island. The ebb runs to the right joined by a small flux from the east side of the gyre and exits northwards along North Channel eastside. There are no major rivers along the Manx west coast or the Northern Irish east coast. Therefore, sea surface temperatures at Port Erin represent waters mainly from the North Channel of subtropical and subpolar origin.

1.3 Surface timeseries data

Kinsman (1957) pointed out the problems of using datasets collected for one purpose then used for another as reported above. The problem of remote bureaucratic data collection was raised in the 1890s when PEMBS was first established in the late 19th century (Herdman, 1893). The issue was: "With an elaborate organisation, such as that

suggested by the Conference, there is a danger that the work of the biological stations would degenerate into the mere taking and recording of routine observations, whilst the original work and the development of new methods of research, which are in reality of far greater importance, would receive a check. Good men would certainly not be attracted to work which consisted merely in recording observations taken according to stereotyped plan dictated by a central bureau. A large amount of individual freedom to the workers is absolutely essential in order to secure the best results from scientific research" (Allen, 1899). PEMBS avoided such problems by having only a few collectors of daily scientific data overseen by active research scientists until the station closed in 2006 (Herdman, 1920; Allen et al., 1998). A data logger continues the SST series at the nearby RNLI station (Fig. 1 inset.)

At Cypris Station (54.2° N, 4.8° W) 5 km SW of Port Erin, collection of depth profiles of temperature, salinity, and various chemical tracers began in 1954 at weekly intervals where possible (Allen et al., 1998). However, it is not a continuous record with daily sampling as at PEMBS, and is therefore less useful for examining physical processes on diurnal timescales (Kinsman, 1957). Indeed, during periods of greatest interest, during sustained storms and gales, there are occasional gaps in the record for a month or more. We are fortunate that the PEMBS daily timeseries continued with methods unchanged for so long.

1.4 Previous oceanographic surface analyses

Sea surface temperature and salinity with respect to Irish Sea tidal circulation including Port Erin SST records were reported from 1902 to 1937 in (Proudman et al., 1937; Proudman, 1946), for 1935–1946 in Gilles (1949), and for 1947–1961 in Hughes (1966). Proudman investigated horizontal surface temperature gradients over a tidal cycle and found maximum values $\sim 1\,^{\circ}\mathrm{C}$ per 20 nm (nautical mile = 1.85 km) (Proudman, 1938). He showed a summer regime established by May with a winter regime by November. An isothermal plot for November clearly shows warm surface waters entering St George's Channel with a cooling gradient into Liverpool Bay. Proudman (1936)

noted that currents in the North Channel had residuals that appeared to be wind-driven after extraction of the strong semidiurnal tidal currents. Earlier work had shown the importance of sustained winds in influencing currents (Proudman and Doodson, 1926).

There is a summary of the temperature and salinity regime off the North European shelf and Irish seas in Huthnance (2010). The main features of the timeseries is an early 20th century warming 1910–1940 of 0.3 °C then steady or slightly declining temperatures until the 1970s followed by a continued rise by 0.4 °C. Source waters for Celtic sea are from southwest of UK with surface waters 9–11 °C in winter and 16–18 °C in summer when stratification is observed. Source waters for North Channel are from the north and west of UK with ranges 9–10 °C in winter and 12–14 °C in summer. Interannual variability exceeds trends over decades that make determining long-term trends difficult. It was also noted that modern monitoring has been sparse in these north Atlantic shelf seas. However, a recent survey of temperature trends near the shelf edge confirms the larger warming trend in air than in SST and that it is more intense north of ∼ 48° N (Holt et al., 2012). The importance of stratification on air/sea exchange was noted and the trends in the centennial Port Erin temperatures well reproduced by the model. The present analysis should add detail to these observations.

The variability of temperature and salinity in the Irish Sea over the 40 yr period 1960–1999 was investigated in some detail using a fine-resolution local area model using the usual 10 m wind formulations (Young and Holt, 2007; Smith, 1988). They found summer warming (May–October) at Cypris of $0.015 \pm 0.008\,^{\circ}\mathrm{C\,yr^{-1}}$ was higher than the modelled results. The winter warming (November–April) of $0.006 \pm 0.008\,^{\circ}\mathrm{C\,yr^{-1}}$ was also higher but much more variable. A 489 yr timeseries of proxy temperatures from long-lived clams showed the seasonal difference between bottom and surface waters narrowed post-1985 from a peak difference of 10 °C (Butler et al., 2010).

The 35 yr, 1960–1994, SST time-series analyses for eight European Shelf Sea sites shows the same trends (Visser et al., 1996). Before 1960, there was insufficient data for time-series analysis. They report that Atlantic water dominates the eastern Irish Sea, the English Channel entrance, the Scottish northeast (NE) coast, and the southwest

(SW) Norwegian coastal waters. However, they considered the southwestern Irish Sea, represented by Cypris Port Erin data, as a separate ecosystem. This is consistent with the tidal gyre amphidromic circulation limits. They used monthly means and interpolations because there were gaps in some records. They did some simulations with a multi-layer numerical model. The surface was simulated for upper 10 m layer centred at 5 m in cell boxes. Of interest here are boxes for the Irish Sea between the Isle of Man and N Wales, the English Channel between Lands End and Brittany, the Scottish North Sea coast and SW Norwegian Coast.

1.5 The 1985–1989 transition

All model results showed a dramatic temperature rise from ∼ 1985–1989 (Visser et al., 1996). The largest rise of ∼ +2 °C was off the Friesian Islands in the German Bight and along the Norwegian Coast off Bergen. The Cypris box had a rise ∼ +0.7 °C, the North Sea coast off Edinburgh ∼ +0.6 °C and English Channel off Lands End ∼ +0.4 °C. Unfortunately the English Channel records ended in 1985. It showed the highest mean temperature of 12.35 ± 2.62 °C for 1962–84 compared with Isle of Man box 10.54 ± 2.49 °C for the decade longer record from 1962–1994. The low variability in salinity suggests different origins with an Isle of Man box-mean of 34.18 ± 0.22 ‰ and the English Channel a more saline 35.20 ± 0.13 ‰ representative of Atlantic water. This is consistent with observations in Celtic Sea gyre.

Trajectories for theoretical particles released at points on the shelf edge at 5 m were modelled for 360 days. Particles released north of Scotland travelled anticlockwise around the North Sea and up the Norwegian coast. This is in accord with normal North Sea cyclonic circulation (Sündermann and Pohlmann, 2011). A particle released north of Malin Head had a similar cyclonic pattern travelling along the Irish coast of the western Irish Sea to cross St George's Channel near Dublin on the south side of the tidal amphidrome gyre and along the North Wales Coast off Menai Strait (Fig. 1b). A particle south of Ireland travelled along the shelf break to round Land Ends into the English Channel. It ended on the French side of Dover Strait. A particle released off Lands End

followed the same route through Dover Strait and ended in the cyclonic North Sea gyre off Jutland. We therefore get a picture of residual currents in cyclonic gyres for the Irish and North Seas. The tidal amphidromy off Port Erin appears to restrict cyclonic ebb and flood mainly to carry water from sub-polar and sub-tropical waters from the North Channel. However, wind-driven currents under SW prevailing winds could carry from St Georges Channel.

The potential future impact of climate change on the hydrography of the northwest European shelf North Sea and the North Atlantic was investigated using coupled ocean and Hadley centre models (Holt et al., 2010). They suggested that by 2100 shelf temperatures could rise from +1.5 °C to 4 °C while salinity could decrease by –0.2 ‰. The model suggested the shelf waters were temperature controlled while the ocean was salinity driven. As we noted earlier both temperature and salinity are important especially in the frontal regions where the impact on density is balance at about 10 °C.

2 Irish Sea and Port Erin sea surface data

Irish Sea SST records have been collected since c1870 for meteorological, fisheries, biological and dynamical oceanographic purposes. Daily noon observations of Irish Sea SST began ∼ 1870 from coastal stations, lighthouses and lightvessels using standard Met Office thermometers to ±1° F (0.6 °C) (Proudman et al., 1937). From 1880, this changed to twice daily at sunrise and 16:00 LT. From ∼ 1900 Irish Sea SST data to ±0.1° F (0.05 °C) were collected for fisheries research, and from 1902 twice daily observations to ±0.5° F (0.3 °C) were taken from PEMBS (Herdman, 1893; Herdman, 1920). Later observers used Nansen bottles with calibrated reversing thermometers to ± 0.01 °C from Port Erin stub of the partially submerged wrecked quay at the entrance to the bay (54.09° N, 4.77° W) (Fig. 1 inset). After PEMBS closed in 2006, the Isle of Man government has continued data collection by automatic data logger at the nearby Royal National Lifeboat Institution lifeboat station (54.09° N, 4.77° W) ∼ 100 m east of the quay with free

deepwater access (http://www.gov.im/categories/the-environment-and-greener-living/isle-of-man-government-laboratory/marine-water-monitoring/). Ronaldsway Isle of Man Airport (54.09° N, 4.63° W) has daily meteorological records from the mid-twentieth century. There are no permanent Irish Sea buoys recording atmospheric and oceanic gradients in temperature and salinity. Irish Met Office Buoys, M2 and M5, record only SST for UK Met Office purposes (Irish Met Office, personal communication, 2013).

3 Results

3.1 Port Erin Marine Biological Station SST 1904–2012

Three distinct periods are immediately obvious from the annual means and polynomial trends shown in Fig. 2a and Table 1. Trend lines are plotted at the centre of each period with means. The 36 yr, 1904–1939, rise of $+0.018\,^{\circ}\mathrm{C\,yr^{-1}}$, followed by 47 yr, 1940–1986, weak mid-century cooling $-0.002\,^{\circ}\mathrm{C\,yr^{-1}}$ and finally the modern 1987–2012 much higher rate of $+0.037\,^{\circ}\mathrm{C\,yr^{-1}}$. The majority, 0.96 °C, of the of 109 yr temperature rise of 1.01 °C took place since 1986. Port Erin has a seasonal cycle as well as shorter and longer cycles. These three periods of warming, slight cooling, then more rapid warming is consistent with earlier observations and our suggested Arctic icemelt phases (Matthews and Matthews, 2013). It confirms the warming trend on the European shelf from late 1980s. It is consistent with the mean 0.6 °C global surface ocean temperature rise over 135 yr from early to modern comparisons UK Challenger 1873–6 and German Meteor 1925–27 (Roemmich et al., 2012; Hobbs and Willis, 2013; Gouretski et al., 2013). The high latitude PEMBS (54° N) location is expected to show polar amplification.

Running means are plotted to the end of each period rather than the normal centred method. This is done to show the current trend from the latest available data. Thus, 30 yr-means are shown time shifted forward by 15 yr and 10 yr-means by 5 yr. Where

there are abrupt shifts, we believe this method is more able to show trends. They show as temperature difference over 1 yr, 5 yr and 15 yr at the current date. Annual running means run from 1904, 10 yr means from 1914, and 30 yr means from 1934. This illustrates how running means change through climate shifts. The temptation to remove deviations from statistical means can therefore be avoided (Kinsman, 1957; Matthews and Matthews, 2012). These trends are not obvious using the usual atmospheric and oceanic climate measure of 30 yr means for fixed periods (e.g. 1970–1999). We suggest a 10 yr running mean ending with the latest data would be more appropriate for demonstrating a rapidly changing climate.

There is a variable cycle of hot and cold years with a period $\sim 8 \pm 2$ yr and amplitude $\sim 1.1 \pm 0.4\,^{\circ}$C. This is similar to the value obtained from spectral analysis by Young and Holt (2007). There is of course a seasonal variation with lows in January/February and highs in August. But it is clear that balance between heat gain and loss is not reached on an annual basis. Thus 8–10 yr-means are appropriate to see long-term trends.

An extraordinary high 1959 to low 1963 event dominates the mid-century slight cooling trend. Annual averages temperatures fell from 11.54 °C to 9.28 °C. It suggests a significant warming event in 1959 and a subsequent extreme cooling to give the extraordinary 2.26 °C temperature difference.

3.2 Cypris Station SST record 1954–2010

Cypris station data from 1954–2010 provides a useful check on the PEMBS data for a shorter period. Correlation between the two records is 0.96. It replicates all features including the 1959–1963 high to low event. It is for a similar period to the 1950–2010 ocean heat content time-series analyses used for modern ocean-warming estimates (Levitus et al., 2012). Figure 2b and table show trends. Annual, 10 yr and 30 yr running means show similar trends to the PEMBS but over emphasise mid-century cooling. This is likely due to the 1959–1963 extreme cycle. The mid-century 33 yr period, 1954–1986, shows a strong downward temperature trend of –0.015 °C yr^{-1}. However, the 26 yr, 1987–2010, warming trend 0.033 °C yr^{-1} completely reverses earlier cooling.

Thus, the overall warming is 1.0 °C for the 57 yr period is the same for both Cypris and PEMBS. However, we note that the Levitus et al. (2012) ocean heat content data is increasingly sparse going backward from 1990 to 1950. We suggest therefore that our daily data is a better long-term indicator of ocean heating trends.

3.3 Comparison with Central England Temperature (CET)

Central England temperature (CET) is the pre-eminent long-term record of air-over-land temperatures (Data Crown Copyright courtesy UK Met Office (http://www.metoffice.gov.uk/hadobs/; Manley, 1974; Parker et al., 1992; Parker and Horton, 2005). CET data are complete from 1659 and a daily record is available from 1904. The nearby Ronaldsway air temperature record is only from 1948 (Hisscott, 2006). Therefore, we use CET for long-term trends. The CET trend since 1900 to 2004 of 0.077 °C per decade is significant at the 1 % level (Parker and Horton, 2005). The record is an average over all the central England landmass to the east of the Isle of Man (Parker, 2013). The CET land-air to PEMBS SST correlation coefficient 1904–2011 is 0.8. This suggests that Central England mainly derives temperatures from the warm Gulf Stream and north Atlantic waters on prevailing SW winds as does PEMBS SST. However, the remaining 20 % in the CET record is probably attributable to continental airflows on short timescales that do not influence the seawater temperatures

The 108 yr CET record shows the same warming-cooling-warming pattern seen in SST (Fig. 2c and Table 3). The 1904–1939 warming rate of +0.015 °C yr^{-1} is only slightly exceeded by the 1987–2011 warming rate +0.018 °C yr^{-1} with a small mid-century cooling from 1940–1986 of −0.004 °C yr^{-1}. The post 1987 warming trend is about half that of the Port Erin sea surface temperature. Hisscott (2006) from analysis of the records from 1948–2006 showed a trend to more coastal fog in summer and less in winter. He reported that air temperature exceeded sea temperature for almost half the year in the first part of the record. However, since 1988 air temperature had been increasing at 0.3 °C per decade while SST increased at 0.6 °C per decade. This results in different seasonal trends in fog climatology. Total CET air warming is only 0.46 °C

that, together with the 1904–1939 0.54 °C warming, contributes to the 0.92 °C 108 yr total. Thus seawater is warmed ∼ 0.1 °C more than land-air over the century. This is consistent with heat accumulating in the oceans. The most striking comparison is that the 1959–1963 hot/cold event is visible in the land air record. For the mid-century CET 1940–1986 the hottest years were 1949 10.6 °C with 1957 s highest at 10.0 °C (Table 3). Indeed March 1957 was the highest March air temperature at 9.2 °C from 1904–2011 (Table 6). This suggests 1957 solar irradiance maximum was felt in the March air anomalous high.

3.4 Mid-twentieth century 1959–1963 hot-to-cold event

The 2.26 °C SST differences over 4 yr suggest an unusually strong warming event in 1959. Water was warmer than long-term averages for 6 months of 1959 (Table 5). It is based on daily readings so systematic errors in monthly means are unlikely. The only source of ocean heat is solar radiation.

Sunspots are very good indicators of solar activity (Solanki, 2003). Sunspots are found at the base of coronal loops. The more sunspots there are the more active the sun. The Photometric Sunspot Index calibrates sunspot numbers to sunspot area and is a widely used as proxy for solar irradiance with records available from 1874 (Balmaceda et al., 2009). De Jager et al. (2010) showed three grand episodes in sunspot numbers. These are the Maunder Minimum from 1630–1721, the regular episode 1721–1923, and the High 20th Century Maximum from 1923–2008. The 20th Century high with maximum 1957–58 is the highest for 400 yr. De Jager and Duhau (2012) predict the next grand episode will be regular and do not expect a Maunder Minimum this millennium. They compared sunspot numbers to land-air surface temperatures and found slowly rising temperatures to 1986. There was increased warming after 1986 as in the CET records. However, the upwards temperature trend coincided the sharp downward trend in solar irradiance/sunspot numbers. This suggests there must be a different mechanism for post-1986 warming.

The period 1904–2012 contains the C20th maximum sunspot number and total irradiance. The mean number of daily sunspots for the period is 60 ± 50 (Fig. 3a). The well known ∼ 11 yr sunspot solar irradiance cycle that is half the 22 yr Hale period is clearly visible. However, the 1957–1958 peak is outstanding with annual mean numbers over 2 standard deviations and maximum numbers 5 standard deviations above the century mean. It is the peak of the 20th century high sunspot episode in the 19th solar cycle since 1750. We narrow the extreme event down with the monthly means from March 1956 – May 1960 2 standard deviations above the mean (Fig. 3b). Monthly means September 1957 to January 1958 were 3 standard deviations above century mean. The overall record number of 355 sunspots was observed on 24 December 1957.

This suggests record high temperatures observed at PEMBS in 1959 derived from warm equatorial water from maximum irradiance September 1957 to January 1958 that travelled on prevailing currents to 54° N. Temperature differences from monthly means for 1940–1986 from May 1956 to March 1964 show the high/low event (Fig. 3c). These show temperatures with daily and seasonal solar cycles averaged out. The century extreme warm month was October 1959 at +1.7 °C above October mean of 12.72 ± 0.56 °C. The observed record high temperature was 15.56 °C during the seasonal peak for 8d from 26 August to 2 September 1959. October 1959 therefore showed maximum temperature above seasonal norm during the month when tropical warm water is seen at Port Erin. A previous high was seen in November 1956 at +1.5 °C above the November mean of 11.06 ± 0.60 °C. This was also at the time of the tropical water maximum. It shows a rapid recovery from a June 1956 minimum –2.0 °C below the June mean of 11.35 ± 0.64 °C. This was at the time of maximum solar radiation. It suggests polar-origin water was present in June but seasonal warming and the subsequent warm tropical water produced the anomalously high temperatures for the period. This suggests that the seasonal cycle usually obscures the influxes of anomalously warm and cold waters from the solar irradiance variations.

We suggest the century maximum radiation anomaly in October 1959 led to the century minimum anomaly in February 1963 −2.5 °C below the February mean of 7.04 ± 0.89 °C. The record cold surface temperatures of 3.5 °C were observed over two days, 6–7 February 1963, after a rapid fall from 5 °C on 2 February. The minimum was at the time of seasonal low temperatures.

We therefore suggest the 1959 record high surface waters travelled through the Arctic to produce the record cold-water flux in 1963 on the global gyre system. The peak irradiance was 24 December 1957 at the winter solstice. Maximum heat capture was in the tropics. The peak warm anomaly reached Port Erin at peak warming season October 1959. This suggests a travel time from the equator of about 21–22 months. Anomalously warm summer peaks in 1960 and 1961 declined to low anomalies by 1962 (Fig. 3c). This parallels the decline in sunspot numbers to the minimum in 1964 (Fig. 3a). We suggest the anomalously warm water of October 1959 passed northwards from 54° N on the 8.5 Sv waterflow to the Arctic and returned as anomalously cold meltwater 3.5 yr later in February 1963 at seasonal low.

Ocean warming was at its most active 1940–1986 during the C20th sunspot/total irradiance maximum. We believe this led to unusually large basal melting of multi-year ice and deep keels of ice islands for overall cooling of surface waters. The 1959/1963 warm/cool event led to suggestions of discrepancies in the mid-century record and that global warming stalled during the period (Matthews, 2012). We suggest that Arctic basal icemelt was continuous through the century with the three phases deriving from the solar maximum leading to the mid-century overall cooling.

3.5 Extreme winters 1916–1917, 1962–1963 and 2010–2011

SST plots for three extreme cold winters are shown in Fig. 4a. British winter 1962–1963 was the coldest in the 20th century (Hirschi and Sinha, 2007). We suggest extraordinary mid century solar irradiance produced unusually large polar meltwaters. Cyclonic circulation is normal in the Irish and North Seas. However, sustained NE winds reverse the normally cyclonic anti-clockwise North Sea circulation from prevailing SW winds

(see Sündermann and Pohlmann, 2011: Fig. 4). The UK CET during this extreme winter resulted from strong cold easterly and northeasterly winds bringing cold Arctic air (Hirschi and Sinha, 2007). Bowden (1956) showed that cold water passed westwards through the shallow English Channel under strong easterly winds. This happened under strong northeasterly in 1963. For the first time in living memory, brackish water from the Baltic froze up to a mile offshore at Herne Bay in the North Sea. Poole harbour on the English Channel coast froze. This suggests the prevailing wind-driven cyclonic circulation reversed and drove cold polar and Baltic waters around British Isles. This included the North Channel to the Isle of Man where record low temperatures were also observed. This is consistent with expected transit times for Baltic water under sustained ENE winds over many days. It is the reverse surface drift currents under sustained SW winds observed by Williamson (1956).

Differences between three 20th and 21st extreme winters can clearly be seen in the daily Port Erin temperatures (Fig. 4a and Table 4). Data for all 3 yr show a temperature fall from 16 November towards maximum winter cooling. The 1916–1917 and 1962–1963 records show a steady fall to minimum temperatures ∼ 3.3 °C on 27 January 1917 and ∼ 3.5 °C 6 February 1963. Thereafter a gradual spring rise is registered. The 2010–2011 winter temperatures remain higher until the spring rise.

We do not have Ronaldsway Met Office 10 m surface winds for 1916–1917 but we have them for 1962–1963. Winds averaging > 25 kt (∼ 15 m s^{-1}) for one or more days (i.e. ∼ two complete 25 h tidal cycles) produce significant residual current reversals. Over a two-day period, 5–6 February 1963, winds reached a record 53 kt from 120° for 3 h on 6 February. This was the final push of cold stratified polar surface waters alongshore that resulted in the record SST low of 3.5 °C on 8 February 1963. This explains the observed cold waters and freezing conditions reported around the southern UK North Sea and English Channel coasts from Baltic brackish water that are similar to brackish Arctic water from meltwater and runoff. All post-1948 20th century extreme winters show a cold anomaly over the N Atlantic and British Isles with a warm anomaly over Baffin Bay (Hirschi and Sinha, 2007). However, the 1962–1963 winter shows an

unusual cold anomaly from the eastern Beaufort Sea diagonally to US Atlantic coast. The N–S meridional jet stream drove cold polar air over North America and to Western Europe (Screen and Simmonds, 2013).

Therefore, the UK 1962–1963 extreme winter derived from the relatively rare combination of both polar-origin surface cold seawater and polar air. The subpolar jet stream was weakened by the extraordinary heating event in 1959 that gave a larger meridional wind component (Toggweiler and Russell, 2008). Thus, the winter of 1962–1963 was an example of NE wind reversal leading to polar water driven southwards.

The 2010–2011 minimum was ~ 6.74 °C on the 19 December 2010. The 21st century extreme regime is clearly warmer and timed differently from C20th extreme winters. The 21st century extreme winter so far is 2010–2011. 11.42 °C on 16 November was followed by a low of 6.74 °C on 19 December. This is much higher and earlier than the C20th extreme lows. Temperature is relatively constant into the spring warming period with no evidence of the warming seen in 20th century extreme years. There is a rapid fall to ~ 7.3 °C in 15 March 2011 from which the spring warming begins. 20th century spring warming begins at the beginning of February. The modern extreme winter cycle is dominated by the higher temperature regime.

3.5.1 Wind-driven surface waters from satellite data 2010–2011

For the winter 2010–2011 SST, we have complete satellite SST coverage (personal communication, reference Høyer and She, 2007). There was a 2.5 °C cooling in 9 days; 11–19 December 2010. There were no winds from the ENE. This may be a remnant of Gulf Stream tropical water with a freshwater surface pool. To test this theory it is necessary to look at salinity values. However, Gulf Stream origin for the buoyant cool plume over tropical saltwater is suggested by the rapid 2.6 °C rise from 7.3 °C to 9.9 °C on 1 January 2011 after 7 days' wind ~ 6.0 m s^{-1} from 268°, the prevailing warm current direction.

Two periods of strong NE winds in January brought unusually cold waters. European Shelf SST images show cold Baltic water leaving the North Sea around Scotland in the

clockwise anticylconic current reversal. Winds of ~ 10 m s^{-1} from 30–70° coincide with lows of 8.5 and 7.6 °C in January SST record. However, winds from 40° averaging > 13–14 m s^{-1} in March–April brought lows of 7.3 °C. This is usually interpreted as the classic negative phase of the North Atlantic Oscillation (NAO) (Wanner et al., 2001). Nevertheless, we suggest polar-origin Baltic and north Atlantic surface water driven by sub-polar meridional jet stream components from northerly and easterly directions are the cause as in the extreme winter 1962–1963 (Hirschi and Sinha, 2007).

The 21st century cold winters are different from 20th century extremes. We see the seasonal warming from early February in the 20th century. Surface water is now a degree warmer until the early April seasonal upward trend. There was a cold winter 1986–1987 in the CET record. However, we suggest this was not severe because SST temperatures were already warmer than earlier in the century.

3.6 10 yr heat cycles

The post-1986 heat content shift is seen in two decadal heat cycles for 1904–1913 and 2004–2013 chosen to remove decadal harmonics (Fig. 4b). The figure shows the total number of degree-days above a decade-average minimum, to quantify annual heat cycles in seawater. The 21st century heating cycle at 1370 degree days is ~ 7 % greater than the decade-averaged 1904–1913 value 1280 degree days. The net century heat imbalance was +90 ± 30 degree days. The 21st century seasonal cycle is clearly warmer with a decadal maximum of 15.2 °C on 22 August and minimum 7.5 °C on 20 February. This compares with the early 20th century cycle with a maximum of 14.2 °C on 13 August and minimum of 6.6 °C on 21 March. The 90 degree day heating imbalance is 0.9 degree days per year and accounts for the mean temperature rise from 10.1 ± 2.5 °C to 11.2 ± 2.6 °C. However, we know that most of the century temperature rise was post-1986. This suggests that the ~ 90 °-day century rate is a likely to be the same for the 25 yr since 1986.

3.7 The 350 yr CET record

The CET record goes back to 1659 and clearly shows that the +0.9 °C 353 yr warming is the same as the 108 yr warming beginning 1901 (Table 6). It is interesting to note that in the 353 yr record, June is the only month that shows zero air temperature trends while all others have increasing trends and overall rises. January shows the largest rise with +1.7 °C with March second largest at +1.5 °C. Polar Amplification is the concept of Arctic warming with the peak warming in the seasonally coldest months. Tropical heating from solar irradiance/sunspot records has been stable for at least the last 400 yr (De Jager et al., 2010). Therefore, a zero change in the month of June at 54° N at the seasonal solar maximum radiation is consistent with observations.

However, February 1947 was the coldest month at −1.9 °C over the 353 yr CET record. The century minimum PEMBS temperatures were for February 1963 at 4.5 °C and March 1947 at 5.18 °C (Table 5). Both 1947 and 1963 are UK extreme cold and snowy years. However, 1963 had both the coldest seawater temperatures and air temperatures suggesting this rare combination contributed to cold conditions on land and along the shore. We suggest the combination of the solar maximum radiation, two orders of magnitude greater than monthly means, accentuated both the mid-century warming 1957–1959 and resulted in maximum ice melt 1962–1963.

3.8 Seasonal temperature and salinity cycles 1982–2007

Eight-year means are used because they average out observed 8 yr harmonics and give two datasets mostly before and after the 1986/87 shift. A clear regime shift is seen in temperature, salinity, density cycles for 20th century period, 1982–1989, and 21st century, 1999–2006 (Fig. 5a, Table 7). The 20th century has a well-defined annual cycle with a higher salinity and temperature during the spring/summer heating phase and lower salinity in fall/winter. Maximum temperatures are in August with minima in February at higher density. Salinity thus follows a clear seasonal circuit.

The 21st century cycle has shifted to higher salinity and temperature but lower density without a well-defined seasonal salinity cycle. However, there are increased anomalous short period intrusions with a range ∼ 0.75 ‰. For example on 8 November we have a warm low salinity intrusion (12.3 °C, 33.7 ‰, 26.6). This is a consistent anomaly in 8 yr means. It suggests surface freshwater remnants over warm saline stratified water from tropical storms are annual events. It suggests travel times are less than one year or survival of coherent Lagrangian watermasses from previous years. Similar water masses are found in eastern and western Pacific freshwater warm pools reported by many observers (e.g. Wijesekera et al., 2005; Matthews and Matthews, 2013). Warm tropical origin moist air masses induce heavy precipitation in contact with polar air in the Iceland/Azores system. It is therefore possible that recent precipitations falling on annual warm water masses are carried on water from a prior year. There was a warm water anomaly in October 1959 about 18 months after the solar maximum tropical heating in June 1958 at the NH tropical high solar radiation.

Toggweiler and Russell (2008) showed that warming since the last glacial maximum will shift and weaken the mean subpolar jet stream from 45–50° N to 50–55° N. This would suggest a tendency at Port Erin, with water over the Malin Sill at ∼ 55° N and remnants from St George's Strait further south to shift towards more warm tropical water. Weather and storm fronts seasonally move north and south. Equinoctial storms are well known as the subpolar jet streams moves south over the Isle of Man. The regime shift from a well-defined seasonal cycle of subtropical and subpolar water to a shift to higher salinity regime with warm and cold intrusions would be consistent with the warming shift.

Water arriving at Port Erin is from a mix of tropical and subpolar water. It is distinct from English Channel and Celtic Sea water as discussed earlier. All reference to high and low anomalies are given in this context. High salinity intrusions for Port Erin at high temperature in September (15.2 °C, 34.2 ‰, 25.2) suggest they are from tropical Gulf Stream and Columbus gyre that moves seasonally north to south. High salinity and low temperature intrusions in January (9.3 °C, 34.4 ‰, 26.5) suggest their origin in

late season tropics cooled by seasonal heat loss. There has been a shift northwards of the tropical/polar water boundary (Toggweiler and Russell, 2008; Årthun et al., 2012). They show the sub-polar jet streams would shift from latitude 45–50° to 50–55°. The Isle of Man at 54° N is in the new range. The polar amplification in Northern Hemisphere weakens the jet stream so that we have more periods of meridional winds as we saw in the wind regime shift. However, our TS cycle shift appears to confirm that the boundary has already reached latitude 54° N. In the SH the shift coincides with the Antarctic circumpolar channel and stronger winds, upwelling and northward driven surface currents at 50° −55° S (Toggweiler and Russell, 2008).

Daily densities 1982–2006 show seasonal variations and extremes for the two regimes (Fig. 5b). Density for 1982–1986 was 26.05 ± 0.5 at 34.02 ‰, 10.1 °C. Twenty years later for 2002–2006 it was 25.87 ± 0.5 at 34.08 ‰, 11.4 °C. The reduced density was due to the 1.3 °C temperature rise offset by the ∼ 0.06 ‰ salinity rise. The second order polynomial trend went through a maximum density around 1994–6. Maximum density on 22 March 1994 was 28.7 at 36.6 ‰, 6.9 °C and on 28 March 1996 was 28.4 at 36.2 ‰, 7.1 °C. These surface salinities are the same as those observed at 3 m in the Central Tropical Pacific (Matthews and Matthews, 2013). They are clearly of tropical origin since evaporation is the only source of salt at the surface. Arctic brine sinks in highly stratified brackish water. They were observed about a month after the usual seasonal low temperature water in January/February. Low salinity water was observed in November about a month after peak temperatures. Low-density water on 10 November 1994 was 23.9 at 31.9 ‰, 12.2 °C, and on 8 November 2005 was 23.2 at 31.0 ‰, 11.2 °C. The warming trend brought tropical surface waters for about ten years after the abrupt post-1986 rapidly rising temperature regime. However, after about 1996 the seasonal regime shifted to balance the seasonal cycle at higher temperatures and salinities. We suggest the regime shift of Toggweiler and Russell (2008) is taking tropical water through the Arctic. The trend suggests more Arctic ice is now melting for a return to the earlier balanced seasonal cycle. We believe this is likely to be basal icemelt of tidewater glaciers.

3.9 20th and 21st century wind regime

Mean 5 yr, 1960–1964 and 2000–2004, wind directions for Ronaldsway for winter/spring and summer/fall show a wind regime shift (Fig. 6). The most notable shift is the ENE winds May–September 2000–2004 not seen in 1960–1964. Sustained winds from this direction reverse normal cyclonic circulation and drive cold surface waters southwards during the important plankton season. However, prevailing SW winds are present in both summer/fall periods suggesting continuance of dominance of Gulf Stream/Columbus gyre tropical waters. They are modified in the later period however by more westerly and northerly component. This would also bring cold waters into the North Channel and result in reduced salinity observed in the TS density plots.

Winter westerlies also appear in both periods. Nevertheless, the 21st century winter westerlies are more frequent. This suggests strengthening of circulation from the Viking polar gyre and transport of more polar water. The wind regime shifts are consistent with reported increase in meridional and zonal components of the sub-polar jet stream (Screen and Simmonds, 2013). This fits well with the observed surface-heating trend and shift to a higher salinity regime while mean salinity is moderated by intrusions of sub-polar water. Moreover, irreversible mass losses from Canadian Archipelago glaciers are now contributing to these cold brackish surface waters (Lenaerts et al., 2013).

This is a similar process to that observed in the North Pacific over the same period where increased SW winds from a similar climate shift enhanced Pacific water and heat influx through Bering Strait (Danielson et al., 2012). The is consistent with the reported link between observed significant summer increases in meridional wave amplitude over Europe, and mid-latitude weather (Screen and Simmonds 2013). The concept of Arctic amplification linked mid-latitude weather from observations of autumn and winter weakened zonal winds, and an increased frequency of blocking north-south jet streams (Francis and Vavrus, 2012; Jeffries et al., 2013; Walsh, 2013). It is consistent with Toggweiler and Russell (2008) shift as suggested above.

3.10 Relationship to 20th and 21st century Arctic ice melt

Rudels (2012) reviewed Arctic Ocean Atlantic exchange circulation and pointed out the importance of the low salinity surface layer outflows to the North Atlantic. Beszczynska-Möller et al. (2011) confirmed changes in recent decades in the two main Arctic Ocean processes of poleward oceanic heat flux and export of freshwater to the North Atlantic. Woodgate et al. (2010) used the observed Bering Strait volume and heat transport between 1991 and 2007 in numerical flow models. In both volume and heat transport 2007 values were record highs; 2007 heat flux ~ 5–$6 \times 10^{20}\,\mathrm{J\,yr^{-1}}$ was twice 2001 measured flux. They suggest interannual flow variability ~ 0.2 Sv. They note that the incoming Pacific Ocean heat flux is sufficient to account for 1/3 seasonal Arctic ice loss or to melt an ice sheet 1 m thick over an area of 1–$2 \times 10^{6}\,\mathrm{km^2}$.

The onset of increased Arctic ice melt coincides with the increased warming of Port Erin surface waters and north European waters in the well-documented shift 1986–1987. Daily mean Arctic sea ice volumes for 1979–1986, 1987–1991, and 2005–2012 are shown Fig. 7. Data are by courtesy of Zhang and Rothrock (2003); http://psc.apl.washington.edu/wordpress/research/projects/arctic-sea-ice-volume-anomaly/data/. The long-term annual melt volume of $\sim 16.2 \times 10^{3}\,\mathrm{km^3}$ was already changing by the second period 1987–91. The period 1986/7 marked warming regime shift as in PEMBS and European SST and CET land-air temperatures.

Net annual reduction in ice volume post 1986 is $-0.4 \times 10^{3}\,\mathrm{km^3}$ shows the observed rapid ice loss. The 8 yr periods 1979–1986 and 2005–2012, ice volume, area and thickness trends are shown in Table 8. The annual ice melt, the difference between maximum and minimum ice volume, increased from 16.2 ± 0.9 to $17.8 \pm 0.9 \times 10^{3}\,\mathrm{km^3\,yr^{-1}}$. It is now melting $\sim 1.6 \times 10^{3}\,\mathrm{km^3\,yr^{-1}}$ more ice than in the previously relatively stable period before 1986. However, the same quantity of heat or more is available now to melt a lower starting volume. This accounts for the higher annual melt rate. As starting volumes continue to decrease there should be heat available for other processes.

It was briefly thought that ice melt had paused based solely on satellite ice area observations. However, Barber et al. (2009) showed that porous rotten annual ice and compact multi-year ice have identical satellite radiometric signals despite have very different melt rates. Only field observation showed the differences in the actual ice. We use ice volume for heat calculations but look at the impacts on ice thickness and area.

The mean volume has changed from the long-term stable volume of $\sim 23 \times 10^{3}\,\mathrm{km^3}$ to $\sim 15 \times 10^{3}\,\mathrm{km^3}$ a reduction of ~ 34 %. This has reduced ice volume $\sim 8 \times 10^{3}\,\mathrm{km^3}$ over the 26 yr period. Heat formerly used in the annual ice melt is now available for additional surface warming of $\sim 2.7 \times 10^{21}$ J (latent heat of fusion $\sim 3.42 \times 10^{8}\,\mathrm{J\,m^{-3}}$) at the rate of $\sim 1 \times 10^{20}\,\mathrm{J\,yr^{-1}}$. There is a positive feedback mechanism of increased summer open water later into the freezeup season and potential for enhanced basal ice melt through the winter. This would tie into the new seasonal density cycles observed at Port Erin (Fig. 4b).

The mean annual maximum to minimum ice melt area over the 8 yr cycles increased from 9.1 ± 0.3 to $10.4 \pm 0.4 \times 10^{6}\,\mathrm{km^2\,yr^{-1}}$ (Table 8). Data are by courtesy of courtesy of http://nsidc.org/data/docs/noaa/g02135_seaice_index/index.html?file=/data/seaice_index/derivation.html *Sea Ice Index*, Boulder, Colorado USA: National Snow and Ice Data Center, Digital media. This suggests a change in ice thickness. We computed the ice thickness from volume/area for the two periods and found the mean ice thickness had decreased by 0.5 m from 1.9 m to 1.4 m (Table 8).

The trends show ice volume reduction rate rose from $0.2 \times 10^{3}\,\mathrm{km^3\,yr^{-1}}$ to $0.7 \times 10^{3}\,\mathrm{km^3\,yr^{-1}}$. However, the mean areal reduction rate only rose from $0.04 \times 10^{6}\,\mathrm{km^2\,yr^{-1}}$ to $0.05 \times 10^{6}\,\mathrm{km^2\,yr^{-1}}$. This is because the maximum area is now increasing at $+0.04 \times 10^{6}\,\mathrm{km^2\,yr^{-1}}$ whereas it formerly fell at about the same rate. We are now having a greater area of thinner ice. This probably reflects the freezing of the brackish low salinity 0–24.7 ‰ surface waters that freeze from 4 °C to –1.7 °C without vertical mixing (Matthews, 1981c). The Arctic Ocean is a stratified estuary receiving ~ 11 % river discharge while accounting for only ~ 1 % of ocean volume over deeper brine layers (Stigebrandt, 1984; McClelland et al., 2012). It is a double estuary with positive alpha

stratification in the surface and negative beta stratification beneath (Carmack, 2007). Both Pacific and Atlantic warm saline waters interleave and cause basal melting.

3.11 Long term stability and centennial change

Our hypothesis is that three phases of ice melt are consistent with the centennial sea surface temperature measurements at Port Erin through the Alpha/Beta stratified system. Buoyant freshwater flux is consistent with observed changes, between 1958–1970 and 1993–1997 at the beginning of the freezeup season, of substantial reduction in multiyear ice > 2 m, an increase in 1–2 m ice and an increase in open water area over the same period from 19 % to 30 % (Yu et al., 2004). It suggests the erosion of deep keel ice had been ongoing at least from the mid-20th century (Polyakov et al., 2012). The sea ice cover had been stable for 1450 yr before the modern rapid reduction (Kinnard et al., 2011). The long-term equilibrium thickness was maintained by an Arctic surface heat flux of $\sim 2\,\mathrm{W\,m^{-2}}$ that compares with the modern Canada Basin, Arctic Ocean heat flux of $\sim 5\,\mathrm{W\,m^{-2}}$ or $\sim 3.5\,\mathrm{W\,m^{-2}}$ over the basin as a whole (Sirevaag et al., 2011).

The long-term effects of warm Pacific water on the Canada basin were hidden for the first half of the 20th Century by the melting of deep ice island and tidewater glaciers > 4 m. Ocean cycles have a very large variation in timescales (Rooth, 1982). Melting of deep ice keels was mentioned as an indicator of climate change as early as 1955 when a deep fjord in the Canadian Northwest Passage became ice-free but plugged by grounded glacier ice at the exit sill (Crary et al., 1955). The Canadian gateway for freshwater transport to Atlantic is increasingly important in 21st century (Beszczynska-Möller et al., 2011). There was a rise in iceberg numbers in Labrador Current crossing 48° N from 1902–1912 with peaks in 1909 and 1912 that ultimately focussed attention on icebergs through Titanic disaster (Diemand, 2001). The mean sea ice extent appeared stable but deep ice erosion appears to have been progressing since about the 1890s.

4 Discussion

4.1 Centennial polar amplification in Northern Hemisphere

Walsh (2013) clearly showed polar amplification of global warming in his study of the Northern Hemisphere. His polar hemisphere surface temperature plot for 1963–2012 is reprinted as Fig. 8. Figure 8 shows warming 1–2 °C during 1963–2012 in the Bering Sea and along the Irish coast ~ 54° N, including the Malin sill and Irish Sea but not the Celtic Sea. We found warming of +1.22 °C for the same period in PEMBS sea surface temperature and a linear trend of $0.026\,^{\circ}\mathrm{C\,yr^{-1}}$. The central North Atlantic from Newfoundland has a temperature rise < 1 °C because of the meltwaters in the eastbound Viking Gyre. We suggest our analysis of the warming at Port Erin shows prevailing SW winds and currents carrying tropical water with intrusions of brackish subpolar meltwaters and runoff water as hypothesised. We showed the NH sequestered 2/3 of surface ocean heat below 3 m in the central tropical Pacific compared with 1/3 in the SH (Matthews and Matthews, 2013). This is not the beta/alpha boundary but a consequence of the southern tropical Pacific hypersalinity (> 36 ‰). The North Atlantic Ocean is less saline than the North Pacific because it carries all the Arctic meltwaters and runoff. These waters travel on Carmack's (2007) downhill (pycnocline) supply of stratified brackish Arctic waters over a deep halocline/pycnocline. Tropical NH Atlantic heat sequestration should be also about 2/3 of ocean surface heat. The circulation of unusually warm water during the mid-20th century peak sunspot/solar irradiance two standard deviations greater than monthly means suggest this is the case. It could be determined from hourly data from meridional transects in the central Atlantic as we used in the central tropical Pacific (Matthews and Matthews, 2013).

4.2 Solar irradiance variation and climate shifts

Equatorial solar irradiance at the equator is year-round in the range = 1–0.9 of total peak irradiance, cosine of angle of incidence ±22.5°. Seasonally in the tropics, latitude

±22.5°, the angle of incidence cosine is in the range 1.0–0.7. Thus, the tropics have year-round solar irradiation in the range 0.7–1.0 of the total incident radiation. In polar regions, year-round heating process derives from basal ice melt from high heat-capacity seawater rather than seasonal weak irradiance. Because of this, tropical heating is the major source of ocean heat. The Pacific Ocean tropics capture the majority of ocean heat (Levitus et al., 2012). However, the Atlantic/Arctic Ocean captures the majority of icemelt in buoyant surface waters. We found warm tropical water reached Port Erin at 54° N about 20 months after the 1957–8 extreme solar radiation event. The Gulf Stream/Columbus subpolar gyre half period is about ~ 20 months. Moreover, seawater density, a function of temperature and salinity, controls ocean heat sequestration (Matthews and Matthews, 2013). The balance point at which the density contributions are equal and opposite is at a surface temperature 10 °C (Carmack, 2007). This is a region of abrupt fronts and where warm saline water comes up against wall of cold polar water (Ebbesmeyer et al., 2011). It is the site for ocean conveyor brine separation. Long-term variations in solar radiation over at least 250 yr did not affect observed anthropogenic global warming (Rohde et al., 2013). Observed land-air warming could be completely explained by top of the atmosphere volcanism and the log of CO_2 concentration. Indeed a sharp increase post-1986 in AGW coincided with a sharp decrease in solar irradiance/sunspot numbers after the 1923–2008 20th century high.

The Viking gyre period is not well defined because of a lack of drifter verification data (C. C. Ebbesmeyer, personal communication, 2013), However, we know from the low salinity anomaly studies based on weather ship observations that cold low salinity anomalies travel from off Greenland to UK in about 4 yr and separate anomalies about a decade apart (Dickson et al., 1988). Modern surface temperatures studies from satellites and instrumented seals suggest the warm and cool waters circulation has intensified in recent years (Hydes et al., 2004; Mernild et al., 2012). Warm tropical water has been observed basal melting tidewater glaciers year-round in East Greenland and focussed attention on the importance of tidewater glaciers (TWG) to global warming (Mernild et al., 2012; Straneo et al., 2013).

The post-1986 climate shift observed in the Arctic/Atlantic appears about a decade earlier in the Pacific. The Pacific Ocean receives the majority of ocean AGW but surface waters are trapped by Bering Strait. It loses only about a tenth of the Atlantic 8.5 Sv into the Arctic Ocean (Beszczynska-Möller et al., 2011). Alaska was not ice covered during the last glacial maximum when Isle of Man was completely ice covered (Fig. 1a). Alaskan tidewater glaciers have been melting since the beginning of the industrial revolution and at least from 1820 (Matthews, 1981a). North Pacific gyres re-circulate heat to produce complex pathways with southbound warm western boundary currents not found in the Atlantic (Fine et al., 1994). Jet stream meridional variations can carry air from the north Pacific over Alaska and south from the Beaufort Sea toward north central USA (Francis and Vavrus, 2012). Wendler and Shulski (2009) reported a rise in Central Alaska air temperatures from 1972–3. Crawford et al. (2007) reported a temperature rise of +0.9 °C from 1958–2005 in the 10–50 m deep layer along Line P through the Aleut subpolar gyre. However, the bulk of Crawford et al.'s (2007) reported temperature rise was in 1977. Moreover, the largest of the 18 climate shifts reported by Douglass (2010) was also in 1976–1977.

4.3 Further potential impacts

There are further impacts of rapid Arctic amplification. Arctic storms are now very similar to mid-latitude storms with great coastal erosion (Simmonds and Rudeva, 2012). There is increasing evidence of Pacific species of flora and fauna entering the Arctic Ocean and some getting established in the North Atlantic. For example, Japanese skeleton shrimp, the Chinese mitten crab and the leathery sea squirt have already reached the British Isles (http://www.marlin.ac.uk/marine_aliens/). King Crabs have reached Norway from Kamchatka and Alaska. We suggest the wind-driven Lagrangian coherent water masses may be important as jet streams of the ocean. Williamson (1957) reported Irish Sea North Channel coherent watermass carrying plankton travelled up to 320 km north to the Minch, Outer Hebrides channel under prevailing strong SW winds. The peak ENE winds May–September 2000–2004 (Fig. 6) could reverse the

flow so that northern species could travel south to the Irish Sea fjord as we observed in the North Channel from NW winds along the channel axis. This is particular significant for bottom species such as starfish that have larval hybridisation where buoyant larvae with bi-lateral geometry metamorphose into benthic animals with circular geometry (Williamson, 2006, 2009, 2012; Williamson and Boerboom, 2012). The long-living Norwegian clams could have travelled this way to the 100 m-deep fjord off Port Erin (Butler et al., 2010).

Ebbesmeyer and Scigliano (2009) noted that Arctic Ocean gyres; Beaufort, Melville, and Polar Bear gyres have travel speeds of 0.6 nm day^{-1} and periods of 12–14 yr. However model and field studies suggest that, in an ice-free ocean, gyre speeds will be as high as 7 nm day^{-1} with much shorter trans-Arctic travel times. This could have far-reaching consequences for ecosystems and circulation patterns.

PEMBS mean SST shifted from $10.24 \pm 0.52\,^{\circ}$C during 1904–39 to $10.8 \pm 0.45\,^{\circ}$C during 1987–2012. A surface temperature of $\sim 10\,^{\circ}$C marks the density balance point where salinity and temperature have equal and opposite effects. It is the sinking front on the global conveyor. Our temperature shift suggests a northward shift in the North Atlantic fontal system. Temperature is a major moderator of ocean carbon dioxide exchange and ocean acidification (Feely et al., 2008; Mathis et al., 2011). Seasonal acidic upwelling from northerly coastal winds along the tidal Pacific Northwest coast has resulted in flushing of oyster beds so that Pacific oysters are unable to spawn naturally since 2007 (Waldbusser et al., 2013). Similar upwelling could accompany the new ENE and N wind regimes in the north Atlantic. Global ocean acidification and sea surface temperature will be discussed in a forthcoming paper (Matthews, 2013). Polar amplification in the Arctic is likely to lead to positive feedback from methane release from quasi-stable methane hydrates at ~ 400 m (Archer et al., 2007). Better understanding of seasonal cycles would aid in determining methane Arctic impact (Kort et al., 2012).

5 Conclusions

We conclude that European North Atlantic AGW at $\sim 54^{\circ}$ N 1987–2012 is increasing at $+0.53\,^{\circ}$C decade^{-1} (i.e. $> 1\,^{\circ}$C in 20 yr) after a century of modification by Arctic basal ice melt. These findings are based on accurate high-quality observational timeseries unaltered by models or data processing. AGW is controlled by top-of-the-atmosphere dynamics and thermodynamics of solar radiation modified by volcanism and greenhouse gases. Ocean AGW is controlled by the top 3 m of ocean dynamics and thermodynamics. Ocean solar radiation heat imbalance is controlled by year-round tropical evaporation and heat sequestration modified by high latitude year-round basal ice melting and seasonal radiative loss restricted by strong stratification. Stratified ocean circulation carries nutrient-rich surface water through the Arctic to the North Atlantic. Surface transport by interconnected wind-driven/geostrophic counter-rotating gyres is strongest in the top 2 m. Eastbound surface gyres make landfall on the west coasts of both north Pacific and north Atlantic at about $\sim 54^{\circ}$ N. PEMBS Isle of Man on the western Irish Sea fjord coast is ideally located to monitor centennial changes from daily timeseries at a fixed location.

We found three phases of surface temperature trends: rising $+0.018\,^{\circ}$C yr^{-1} during 1904–1939, slight falling $-0.002\,^{\circ}$C yr^{-1} during 1940–1986, and more than double the early C20th rising at $+0.037\,^{\circ}$C yr^{-1} during 1987–2012. This is consistent with three phases of Arctic ice melt: first the deep keels of tidewater glaciers and ice islands, second the multiyear ice and now the modern annual ice. The C20th sunspot/solar irradiance maximum that peaked in 1957 resulted in a large heat anomaly in October 1959. That heating event carried on the 8.5 Sv flux between Scotland and Greenland to the Arctic resulted in unusually large ice melt and cold water at Port Erin in February 1963. Irradiance during the 1923–2008 solar maximum of at least two standard deviations larger than monthly means resulted in the 1959/63 hot/cold event. We suggest unusually large tropical warming led to unusually large basal Arctic melting that reached Isle of Man ~ 3.5 yr later. We believe this accounts for record cold European 1962/3 winter

and century extreme cold sea surface temperatures. It confirms the suggestion that basal icemelt is the principal cause of observed Arctic thermodynamic processes.

Post-1986 we found surface water and wind regime shifts. Surface water ceased a regular TS seasonal cycle. It now has ~0.18 lower mean density from ~1.3 °C higher temperature modified by ~0.06 ‰ higher salinity. Seasonal density minimum is in November and maximum in March. Intrusions of high and low-density tropical and polar waters were observed. They were carried on Lagrangian wind-drift/geostrophic surface currents driven by winds maintained for ~2 days or more. The wind regime May–September 2004 showed more ENE winds and weakened prevailing southwesterlies. While October–April 2004 showed strong westerly, and weaker ESE wind regime. The 2010–2011 winter low shifted to minimum temperatures March/April.

Modern ocean AGW depends on seawater density and heat trapped mainly in the tropics in the upper 2 m. Total AGW for the last 250 yr can be modelled on volcanism and the log of CO_2 concentration at the top of the atmosphere. Oceans account for 93 % of observed AGW. PEMBS warming during 1987–2012 of $+0.037\,^{\circ}\mathrm{C\,yr^{-1}}$ is representative of ocean warming, formerly buffered by Arctic icemelt, now showing a rapidly increasing trend in sea surface temperatures. Land-air, CET, warming during 1987–2012 ($+0.018\,^{\circ}\mathrm{C\,yr^{-1}}$) is similar to 1904–1940 ($+0.015\,^{\circ}\mathrm{C\,yr^{-1}}$) but is representative only of the 7 % AGW in the atmosphere.

The observations are consistent with Arctic ice melt rate shift to increased melting 2005–2012 of $0.73 \times 10^3\,\mathrm{km^3\,yr^{-1}}$ from the 1979–1986 rate of $0.18 \times 10^3\,\mathrm{km^3\,yr^{-1}}$. This led to more open-water and larger amounts of brackish cold surface water over strong double haloclines. The Arctic Ocean is strongly stratified over deep haloclines from the Atlantic, Pacific, and deeper brine from the freezing process. Year-round basal icemelt can reduce observed mean ice thickness by 0.5 m from 1.9 m 1979–86 to 1.4 m 2005–2012. The modern (2005–12) maximum ice area increasing trend of $+0.4 \times 10^6\,\mathrm{km^3\,yr^{-1}}$ suggests more surface ice from brackish surface waters $< 4\,^{\circ}\mathrm{C}$ and < 24.7 ‰ that form a stable stratified surface layer.

We found additional heat, formerly absorbed in annual icemelt of $\sim 2.7 \times 10^{21}$ J increasing at $\sim 1 \times 10^{20}\,\mathrm{J\,yr^{-1}}$, is available to increase near-surface water temperatures and melt tidewater glaciers. This is likely to lead to increased sealevels that have been stable for 4000 yr. It is not surprising, given the processes quantified here, to find that actual Arctic sea ice retreat is far ahead of all model projections (Stroeve et al., 2012). Thus, a full understanding of the heat exchange processes cannot proceed without better data on the dynamics and thermodynamics in the top 3 m verified by extensive ground truth fieldwork.

We suggest that far from a lull in global warming, as suggested by atmospheric studies, AGW is proceeding at an alarmingly rapid rate in the oceans as suggested by others (e.g. Hansen, 2009). Clearly, more observational studies are required. Surface satellite data and models are insufficient to quantify global heat balance through the thin ocean boundary layer with its many diverse processes and impacts. North Atlantic drifter studies and daily and hourly meridional timeseries in the top 2–3 m are needed for testing our hypothesis. Nutrient and plankton sampling along with CO_2 and pH are of great importance. We suggest adaptive management of focussed multidisciplinary scientific research on the top 3 m oceans is the most cost-effective method for future work (Matthews and Matthews, 2013b).

Acknowledgements. J. B. R. Matthews is grateful to the Isle of Man government and Andrew Weaver for student support. We thank Dave Brown, Ronaldsway Met Office, for meteorological records and Kevin Kennigton, Manx Government Monitor, for the SST records and UK Met Office for CET records (http://www.metoffice.gov.uk/hadobs/hadcet/), Jacob Høyer of Danish Met Office for providing video clips of the 2010–11-winter SST regime and Don Williamson for discussions and comments on an early draft. We are indebted to John Huthnance for going well beyond the usual role of Topic Editor in order to clarify the paper as a valued colleague to benefit the scientific discussion process. J. B. Matthews records his gratitude for discussions over many years with colleagues: on geophysics problems with Malcolm G. Haines, David G. Fearn, Blair Kinsman, James E. McDonald, G. I. Taylor, B. J. Mason, P. V. Hobbs, Ben Herman, and Louis Battan, on tides and modelling with Norman S Heaps, and Geoffrey Lennon, on fjords with G. L. Pickard, on arctic circulation and ice with Lyn Lewis, Steve Neshyba, Sigmund Kowalik, and

Knut Aagaard, and on multidisciplinary science and adaptive management with Dixie Lee Rae, Taivo Laevastu, John Noye, Daniel B. Hawkins, Donald A. Thomson, Carl Walters and Gunter Weller. The members of SCOR/IAPSO/ECOR/UNESCO Working Group 57 on coastal and estuarine regimes and modelling, of whom JBM was Chairman, were invaluable in broadening and deepening his understanding of geophysical processes and experimental method. Nina Matthews' assistance and proof reading are gratefully acknowledged. This research was self-funded.

References

Aagaard, K. and Carmack, E.: The role of sea-ice and other freshwater in the Arctic Circulation, J. Geophys. Res., 94, 14485–14498, doi:10.1029/JC094iC10p14485, 1989.

Aberson, S. D.: Regimes and cycles in tropical cyclone activity in the north Atlantic, B. Am. Meteorol. Soc., 90, 39–43, doi:10.1175/2008BAMS2549.1, 2009.

Allen, E. J.: The Stockholm Fisheries Conference, Nature, 61, 1568, doi:10.1038/061054b0, 1899.

Allen, J. R., Slinn, D. J., Shammon, T. M., Hartnoll, R. G., and Hawkins, S. J.: Evidence for eutrophication of the Irish Sea over four decades, Limnol. Oceanogr., 43, 1970–1974, 1998.

Andreu-Burillo, I., Holt, J., Proctor, R., Annan, J. D., James, I. D., and Prandle, D.: Assimilation of sea surface temperature in the POL Coastal Ocean Modelling System, J. Marine Syst., 65, 27–40, 2007.

Archer, D.: Methane hydrate stability and anthropogenic climate change, Biogeosciences, 4, 521–544, doi:10.5194/bg-4-521-2007, 2007.

Årthun, M., Nicholls, K. W., Makinson, K., Fedak, M. A., and Boehme, L.: Seasonal inflow of warm water onto the southern Weddell Sea continental shelf, Antarctica, 39, L17601, doi:10.1029/2012GL052856, 2012.

Balmaceda, L. A., Solanki, S. K., Krivova, N. A., and Foster, S.: A homogeneous database of sunspot areas covering more than 130 years, J. Geophys. Res., 114, A07104, doi:10.1029/2009JA014299, 2009.

Barber, D. G., Galley, R., Asplin, M. G., De Abreu, R., Warner, K.-A., Pućko, M., Gupta, M., Prinsenberg, S., and Julien, S.: Perennial pack ice in the southern Beaufort Sea

was not as it appeared in the summer of 2009, Geophys. Res. Lett., 36, L24501, doi:10.1029/2009GL041434, 2009.

Barton, E. D., Inall, M. E., Sherwin, T. J., and Torres, R.: Lagrangian studies of the Iberian upwelling system: vertical structure, turbulent mixing and fluxes during Lagrangian observations of an upwelling filament system off Northwest Iberia, Prog. Oceanogr., 51, 249–267, doi:10.1016/S0079-6611(01)00069-6, 2001.

Basso, D., Bernasconi, M. P.; Robba, E., and Marozzo, S.: Environmental evolution of the Marsala Sound, Sicily, during the last 6000 years, J. Coastal Res., 24, 177–197, doi:10.2112/05-0619.1, 2008.

Beszczynska-Möller, A., Woodgate, R. A., Lee, C., Melling, H., and Karcher, M.: A synthesis of exchanges through the main oceanic gateways to the Arctic Ocean, Oceanography, 24, 82–99, doi:10.5670/oceanog.2011.59, 2011.

Bond, G., Showers, W., Cheseby, M., Lotti, R., Almasi, P., deMenocal, P., Priore, P., Cullen, H., Hajda, I., and Bonani, G.: A pervasive millennial-scale cycle in North Atlantic Holocene and glacial climates, Science, 278, 1257–1266, doi:10.1126/science.278.5341.1257, 1997.

Bowden, K. F.: The flow of water through the straits of Dover, related to wind and differences in sea level, Philos. T. R. Soc. A, 248, 517–551, 1956.

Brown, J., Carrillo, L., Fernand, L., Horsburgh, K. J., Hill, A. E., Young, E. F., and Medler, K. J.: Observations of the physical structure and seasonal jet-like circulation of the Celtic Sea and St. George's Channel of the Irish Sea, Cont. Shelf Res., 23, 533–561, 2003.

Butler, P. G., Richardson, C. A., Scourse, J. D., Wanamaker, A. D., Shammon, T. M., and Bennell, J. D.: Marine climate in the Irish Sea, analysis of a 489-year marine master chronology derived from growth increments in the shell of the clam Arctica islandica, Quaternary Sci. Rev., 2913–2914, doi:10.1016/j.quascirev.2009.07.010, 2010.

Carmack, E. C.: The alpha/beta ocean distinction: a perspective on freshwater fluxes, convection, nutrients, and productivity in high-latitude seas, Deep-Sea Res., 54, 2578–2598, doi:10.1016/j.dsr2.2007.08.018, 2007.

Cook, J.: Ice Age Art: Arrival of the Modern Mind, British Museum Press, ISBN: 978-0-7141-2333-2, 288 pp., 2013.

Crary, A. P., Kulp, J. L., and Marshall, E. W.: Evidences of climatic change from ice island studies, Science, 122, 1171–1173, 1955.

Crawford, W., Galbraith, J., and Bolingbroke, N.: Line P ocean temperature and salinity, 1956–2005, Prog. Oceanogr., 75, 161–178, 2007.

Cunliffe, B.: The Oxford Illustrated History of Prehistoric Europe, Oxford University Press, ISBN: 978-0-19-285441-4, 523 pp., 1997.
Cunliffe, B.: Europe between the oceans 9000BC-AD1000, Yale University Press, ISBN: 978-0-300-17086-3, 518 pp., 2008.
Dabrowski, T., Hartnett, M., and Olbert, A. I.: Influence of seasonal circulation on flushing of the Irish Sea, Mar. Pollut. Bull., 60, 748–758, 2010.
Danielson, S., Hedstrom, K., Aagaard, K., Weingartner, T., and Curchitser, E.: Wind-induced reorganization of the Bering shelf circulation, Geophys. Res. Lett., 39, L08601, doi:10.1029/2012GL051231, 2012.
Dat, C. G., Leblond, P. H., Thomson, K. A., and Ingraham Jr, W. J.: Computer simulations of homeward-migrating Fraser River sockeye salmon: is compass orientation a sufficient direction-finding mechanism in the north-east Pacific Ocean?, Fish. Oceanogr., 4, 209–216, doi:10.1111/j.1365-2419.1995.tb00144.x, 1995.
Davies, A. M., Hall, P., Howarth, M. J., and Knight, P: Modelling and measuring the wind forced inflow to the Irish Sea through the North Channel, Cont. Shelf Res., 22, 749–777, 2002.
De Jager, C. and Duhau, S.: Sudden transitions and grand variations in the solar dynamo, past and future, J. Space Weather Space Clim., 2, 1–8, doi:10.1051/swsc/2012008, 2012.
De Jager, C., Duhaub, S., and van Geel, B.: Quantifying and specifying the solar influence on terrestrial surface temperature, J. Atmos. Sol-Terr. Phy., 72, 926–937, doi:10.1016/j.jastp.2010.04.011, 2010.
Dickson, R. R., Meincke, J., Malmberg, S.-A., and Lees, A. J.: The “Great Salinity Anomaly” in the Northern North Atlantic 1968–1982, Prog. Oceanogr., 20, 103–151, 1988.
Dickson, R., Rudels, B., Dye, S., Karcher, M., Meincke, J., and Yashayaev, I.: Current estimates of freshwater flux through Arctic and subarctic seas, Prog. Oceanogr., 73, 210–230, doi:10.1016/j.pocean.2006.12.003, 2007.
Diemand, D.: Icebergs, Enc, Ocean Sciences, 2nd Edn., 181–190, doi:10.1016/B978-012374473-9.00002-3, 2001.
Doodson, A. T.: The tides and work of the tidal institute, Liverpool, Geogr. J., 63, 134–147, 1924.
Douglass, D. H.: Topology of Earth’s climate indices and phase-locked states, Phys. Lett. A, 374, 4164–4168, doi:10.1016/j.physleta.2010.08.025, 2010.
Douglass, D. H. and Knox, R. S.: Ocean heat content and Earth’s radiation imbalance, II. Relation to climate shifts, Phys. Lett. A, 376, 1226, doi:10.1016/j.physleta.2012.02.027, 2012.

Downes, C. R.: History of the British ocean weather ships, Marine Observer, 47, 179–186, 1977.
Ebbesmeyer, C. and Scigliano, E.: Flotsametrics and the floating world, Harper Collins Pub. Co., ISBN 978-0-06-155841-2, 2009.
Ebbesmeyer, C. C., Belkin, I. M., Drost, H. E., Zimmermann, S., and Carmack, E. C.: Wall across the Atlantic: Drift bottles released by students confirm that the Gulf Stream prevents subarctic surface drifters from escaping south, Oceanography, 24, 172–174, doi:10.5670/oceanog.2011.15, 2011.
Ebbesmeyer, C. C., Ingraham, W. J., Jones, J. A., and Donohue, M. J.: Marine debris from the Oregon Dungeness crab fishery recovered in the Northwestern Hawaiian Islands: identification and oceanic drift paths, Mar. Pollut. Bull., 65, 69–75, doi:10.1016/j.marpolbul.2011.09.037, 2012.
Feely, R. A., Sabine, C. L., Hernandez-Ayon, J. M. Ianson, D., and Hales, B.: Evidence for Upwelling of corrosive “acidified” water onto the continental shelf, Science, 320 1490–1492, doi:10.1126/science.1155676, 2008.
Fine, R. A., Lukas, R., Bingham, F. M., Warner, M. J., and Gammon, R. H.: The western equatorial Pacific: a water mass crossroads, J. Geophys. Res.-Oceans, 99, 25063–25080, doi:10.1029/94JC02277, 1994.
Forbes, E.: A History of British Starfishes, and Other Animals of the Class Echinodermata, 267 pp., J. Van Voorst, London, 1841.
Francis, J. A. and Vavrus, S. J.: Evidence linking Arctic amplification to extreme weather in mid-latitudes, Geophys. Res. Lett., 39, L06801, doi:10.1029/2012GL051000, 2012.
Gebbie, G.: Tracer transport timescales and the observed Atlantic-Pacific lag in the timing of the Last Termination, Paleoceanography, 27, PA3225, doi:10.1029/2011PA002273, 2012.
Gilles, D. C.: The temperature and salinity of the surface waters of the Irish Sea for the period 1935–1946, Geophys. J. Int., 5, 374–397, 1949.
Gouretski, V., Jungclaus, J. H., and Haak, H.: Revisiting the Meteor 1925–1927 hydrographic dataset reveals centennial full-depth changes in the Atlantic Ocean, Geophys. Res. Lett., 40, 2236–2241, doi:10.1002/grl.50503, 2013.
Hansen, J.: Storms of My Grandchildren: The Truth About the Coming Climate Catastrophe and Out Last Chance to Save Humanity, Bloomsbury, NY, ISBN 978-1-60819-200-7, 304 pp., 2009.

Herdman, W. A.: Sixth annual report of the Liverpool Marine Biological Committee, and their Biological Station at Port Erin (Isle of Man), Proc. Liverpool Biological Soc., Dobb & Co. Liverpool, available at: http://www.isle-of-man.com/manxnotebook/maritime/mbs/text.htm (last access: 24 December 2013), 1893.
Herdman, W. A.: Thirty-third Annual Report of the Liverpool Marine Biology Committee and their Biological Station at Port Erin and Appendix A, The History and work of the L. M. B. C., Proc. Liverpool Biological Soc., 34, 11–22 and 23–75, 1920.
Hill, E., Durazo, R., and Smeed, D. A.: Observations of a cyclonic gyre in the western Irish Sea, Cont. Shelf Res., 14, 479–490, 1994.
Hirschi, J. J.-M. and Sinha, B.: Negative NAO and cold Eurasian winters: how exceptional was the winter of 1962/1963?, Weather, 62, 43–48, doi:10.1002/wea.34, 2007.
Hisscott, A.: Trends in seasonal occasions of fog at Ronaldsway, Isle of Man, Weather, 61, 202–205, doi:10.1256/wea.229.05, 2006.
Hobbs, W. R. and Willis, J. K.: Detection of an observed 135-year ocean temperature change from limited data, Geophys. Res. Lett., 40, 2252–2258, doi:10.1002/grl.50370, 2013.
Holt, J., Wakelin, S., Lowe, J., and Tinker, J.: The potential impacts of climate change on the hydrography of the northwest European continental shelf, Prog. Ocean., 86, 361–379, doi:10.1016/j.pocean.2010.05.003, 2010.
Holt, J., Hughes, S., Hopkins, J., Wakelin, S. L., Holliday, N. P., Dye, S., González-Pola, C., Hjøllo, S. S., Mork, K. A., Nolan, G., Proctor, R., Read, J., Shammon, T., Sherwin, T., Smyth, T., Tattersall, G., Ward, B., and Wiltshire, K.: Multi-decadal variability and trends in the temperature of the northwest European continental shelf: a model-data synthesis, Prog. Oceanogr., 106, 96–117, doi:10.1016/j.pocean.2012.08.001, 2012.
Horsburgh, K. J. and Hill, A. E.: A three-dimensional model of density-driven circulation in the Irish Sea, J. Phys. Oceanogr., 33, 343–365, doi:10.1175/1520-0485(2003)033<0343:ATDMOD>2.0.CO;2, 2003.
Horsburgh, K. J., Hill, A. E., Brown, J., Fernand, L., Garvine, R. W., and Angelico, M. M. P.: Seasonal evolution of the cold pool gyre in the western Irish Sea, Prog. Oceanogr., 46, 1–58, doi:10.1016/S0079-6611(99)00054-3, 2000.
Høyer, J. L. and She, J.: Optimal interpolation of sea surface temperature for the North Sea and Baltic Sea, J. Marine Sys., 65, 176–189, 2007.
Hughes, P.: The temperature and salinity of the surface waters of the Irish Sea for the period 1947–61, Geophys. J. Roy. Astr. S., 10, 421–435, 1966.

Huthnance, J.: Temperature and salinity, in: Charting the Progress 2: Ocean processes feeder report, section 3.2., edited by: Buckley, P., Connor, D., Cook., D., Cox., M., Dale, T., Dye, S., Frost, M., Hawkridge, J., Huthnance, J., Kroeger, S., Law, R., McKie, J., Maes, T., Malcolm, S., Moffat, C., Moxon, R., Raymond, K., Saunders, J., Vincent, C., Walker, G., Waldock, M., and Williamson, P., London, DEFRA, UKMMAS, 39–106, available at: http://chartingprogress.defra.gov.uk/feeder/Section_3.2_Temperature_and_Salinity.pdf (last access: 24 December 2013), 2010.
Hydes, D. J., Gowen, R. J., Holliday, N. P., Shammon, T., and Mills, D.: External and internal control of winter concentrations of nutrients (N, P and Si) in north-west European shelf seas, Estuar. Coast Shelf S., 59, 151–161, doi:10.1016/j.ecss.2003.08.004, 2004.
Ingraham Jr., J.: Getting to know OSCURS, REFMS's Ocean Surface Current Simulator, Status of Stocks and Multispecies, Quarterly Report, Alaska Fisheries Science Center, June 1997, available at: http://www.afsc.noaa.gov/REFM/docs/oscurs/get_to_know.htm (last access: 24 December 2013), 1997.
Ingraham, W. J., Ebbesmeyer, C. C., and Hinrichsen, R. A.: Imminent Climate and Circulation Shift in Northeast Pacific Ocean Could Have Major Impact on Marine Resources, Eos Trans. Am. Geophys. Union, 79, 197–201, doi:10.1029/98EO00142, 1998.
Isserlin, J. and Taylor, J. du P.: Motya, A Phoenician and Carthaginian city in Sicily, Fieldwork and excavation, 117 pp., Brill, Leiden, 1974.
Jacobs, J.: The story of geographic discovery; how the world become known, eBook #14291, Project Gutenberg, available at: http://www.gutenberg.org/files/14291/14291-h/14291-h.htm (last access: 24 December 2013), 2004.
Jeffries, M. O., Overland., J. E., and Perovich, D. K.: The Arctic shifts to a new normal, Phys. Today, 66, 35–40, doi:10.1063/PT.3.2147, 2013.
Jones, J. E. and Davies, A. M.: Processes influencing storm-induced currents in the Irish Sea, J. Phys. Ocean, 33, 88–104, doi:10.1175/1520-0485(2003)033(0088:PISICI)2.0.CO;2, 2003.
Kennett, D. J., Kennett, J. P., West, G. J., Erlandson, J. M., Johnson, J. R., Hendy, I. L., West, A., Culleton, B. J., Jones, T. L., and Stafford, T. W. Jr.: Wildfire and abrupt ecosystem disruption on California's Northern Channel Islands at the Ållerød–Younger Dryas boundary (13.0–12.9 ka), Quaternary Sci. Rev., 27, 2530–2545, doi:10.1016/j.quascirev.2008.09.006, 2008.
Kinnard, C., Zdanowica, C. M., Fisher, D. A., Isaksson, E., de Vernal, A., and Thompson, L.: Reconstructed changes in Arctic sea ice over the past 1450 years, Nature, 470, 509–512, doi:10.1038/nature10581, 2011.

Kinsman, B.: Proper and improper use of statistics in geophysics, Tellus, 9, 408–418, doi:10.1111/j.2153-3490.1957.tb01897.x, 1957.
Knight, P. J. and Howarth, M. J.: The flow through the north channel of the Irish Sea, Cont. Shelf Res., 19, 693–716, 1999.
Kort, E. A., Wofsy, S. C., Daube, B. C., Diao, M., Elkins, J. W., Gao, R. S., Hintsa, E. J., Hurst, D. F., Jimenez, R., Moore, F. L., Spackman, J. R., and Zondlo, M. A.: Atmospheric observations of Arctic Ocean methane emissions up to 82° North, Nat. Geosci., 5, 318–321, doi:10.1038/NGEO1452, 2012.
Lavender-Law, K., Morét-Ferguson, S., Maximenko, N. A., Proskurowski, G., Peacock, E. E., Hafner, J., and Reddy, C. M.: Plastic accumulation in the North Atlantic Subtropical Gyre, Science, 329, 1185–1188, doi:10.1126/science.1192321, 2010.
Lenaerts, J. T. M., van Angelen, J. H., van den Broeke, M. R. Gardner, A. S., Wouters, B., and van Meijgaard, E.: Irreversible mass loss of Canadian Arctic Archipelago glaciers, Geophys. Res. Lett., 40, 870–874, doi:10.1002/grl.50214, 2013.
Levitus, S., Antonov, J. I., Boyer, T. P., Baranova, O. K., Garcia, H. E., Locarnini, R. A., Mishonov, A. V., Reagan, J. R., Seidov, D., Yarosh, E. S., and Zweng, M. M.: World ocean heat content and thermostatic sea level change (0–2000 m), 1955–2010, Geophys. Res. Lett., 39, L10603, doi:10.1029/2012GL051106, 2012.
Lin, J., Brunner, D., Gerbig, C., Stohl, A., Luhar, A., and Webley, P. (Eds): Lagrangian Modelling of the Atmosphere, Geoph. Monog. Series Vol. 200, AGU, Washington, DC, USA, 2013.
Lumpkin, R. and Johnson, G. C.: Global ocean surface velocities from drifters: Mean, variance, El Nino – Southern Oscillation response, and seasonal cycle, J. Geophys. Res.-Oceans, 118, 2992–3006, doi:10.1002/jgrc.20210, 2013.
Manley, G.: Central England temperatures: Monthly means 1659 to 1973, Q. J. Roy. Meteor. Soc., 100, 389–405, doi:10.1002/qj.49710042511, 1974.
Mathis, J. T., Cross, J. N., and Bates, N. R.: The role of ocean acidification in systemic carbonate mineral suppression in the Bering Sea, Geophys. Res. Lett., 38, L19602, doi:10.1029/2011GL048884, 2011.
Matthews, J. B.: Sicily 1962, Exploration Review, Journal of Imperial College Exploration Society, 4, 39–41, 1963.
Matthews, J. B.: The seasonal circulation of the Glacier Bay, Alaska fjord system, Estuar. Coast Shelf S., 12, 679–700, doi:10.1016/S0302-3524(81)80065-5, 1981a.

Matthews, J. B.: Observations of surface and bottom currents in the Beaufort Sea near Prudhoe Bay, Alaska, J. Geophys. Res.-Oceans, 86, 6653–6660, doi:10.1029/JC086iC07p06653, 1981b.
Matthews, J. B.: Observations of under-ice circulation in a shallow lagoon in the Alaskan Beaufort Sea, Ocean Manage., 6, 223–234, doi:10.1016/0302-184X(81)90040-8, 1981c.
Matthews, J. B. and Matthews, J. B. R: Physics of the upper ocean, Physics Today, under review, 2013.
Matthews, J. B. and Quinlan, A. V.: Seasonal characteristics of water masses in muir inlet, a Fjord with Tidewater Glaciers, J. Fish. Res. Board Can., 32, 1693–1703, 1975.
Matthews, J. B. R.: Comparing historical and modern methods of Sea Surface Temperature measurement – Part 1: Review of methods, field comparisons and dataset adjustments, Ocean Sci. Discuss., 9, 2951–2974, doi:10.5194/osd-9-2951-2012, 2012.
Matthews, J. B. R.: Seasonal variability of sea surface carbonate chemistry and temperature, PhD Thesis, available at: http://dspace.library.uvic.ca:8080/handle/1828/5104 (last access: 1 January 2014), 2013.
Matthews, J. B. R. and Matthews, J. B.: Comparing historical and modern methods of Sea Surface Temperature measurement – Part 2: Field comparison in the Central Tropical Pacific, Ocean Sci. Discuss., 9, 2975–3019, doi:10.5194/osd-9-2975-2012, 2012.
Maximenko, N., Hafner, J., and Niiler, P.: Pathways of marine debris derived from trajectories of Lagrangian drifters, Mar. Pollut. Bull., 65, 51–62, doi:10.1016/j.marpolbul.2011.04.016, 2012.
McClelland, J. W., Holmes, R. M., Dunton, K. H., and Macdonald, R. W.: The Arctic ocean estuary, Estuar. Coast., 35, 353–368, doi:10.1007/s12237-010-9357-3, 2012.
Mei, W., Pasquero, C., and Primeau, F.: The effect of translation speed upon the intensity of tropical cyclones over the tropical ocean, Geophys. Res. Lett., 39, L07801, doi:10.1029/2011GL050765, 2012.
Mellersh, H. E. L.: FitzRoy of the Beagle, Mason & Lipscomb Pub., New York, NY, USA, 1974.
Mernild, S. H., Seidenkrantz, M.-S., Chylek, P., Liston, G. E., and Hasholt, B.: Climate-driven fluctuations in freshwater flux to Sermilik Fjord, East Greenland, during the last 4000 years, Holocene, 22, 155, doi:10.1177/0959683611431215, 2012.
Mungall, J. C. H. and Matthews, J. B.: The M_2 tide of the Irish Sea: hourly configurations of the sea surface and of the depth-mean currents, Estuar. Coast Mar. Sci., 6, 55–74, 1978.

Murton, J. B., Bateman, M. D., Dallimore, S. R., Teller, J. T., and Yang, Z.: Identification of younger dryas outburst flood path from Lake Agassiz to the Arctic Ocean, Nature, 464, 740–743, doi:10.1038/nature08954, 2010.

Olbert, A., Hartnett, M., Dabrowski, T. and Mikolajewicz, U.: Long-term inter-annual variability of a cyclonic gyre in the western Irish Sea, Cont. Shelf Res., 31, 1343–1356, doi:10.1016/j.cr.2011.05.010, 2011.

Parker, D.: Central England Temperature (CET), Weather, 68, 111, doi:10.1002/wea.2111, 2013.

Parker, D. E. and Horton, E. B.: Uncertainties in the central England temperature 1878–2003 and some improvement to the maximum and minimum series, Int. J. Climate, 25, 1173–1188, doi:10.1002/joc.1190, 2005.

Parker, D. E., Legg, T. P., and Folland, C. K.: A new daily Central England Temperature Series, Int. J. Climate, 12, 317–342, doi:10.1002/joc.3370120402, 1992.

Peacock, T. and Haller, G.: Lagrangian coherent structures: the hidden skeleton of fluid flows, Phys. Today, 66, 41–47, doi:10.1063/PT.3.1886, 2013.

Perez, R. C., Cronin, M. F., and Kessler, W. S.: Tropical Cells and a Secondary Circulation near the Northern Front of the Equatorial Pacific Cold Tongue, J. Phys. Oceanogr., 40, 2091–2106, doi:10.1175/2010JPO4366.1, 2010.

Pike, A. W. G., Gilmour, M., Pettitt, P., Jacobi, R., Ripoll, S., Bahn, P., and Muñoz, F.: Verification of the age of the Palaeolithic cave art at Creswell Crags, UK, J. Archaeol. Sci., 32, 1649–1655, doi:10.1016/j.jas.2005.05.002, 2005.

Polyakov, I. V., Walsh, J. E., Kwok, R.: Recent Changes of Arctic Multiyear Sea Ice Coverage and the Likely Causes, B. Am. Meteorol. Soc., 93, 145–151, doi:10.1175/BAMS-D-11-00070.1, 2012.

Post, A., O'Neel, S., Motyka, R. J., Streveler, G.: A complex relationship between calving glaciers and climate, Eos, Trans. AGU, 92, 305–306, doi:10.1029/2011EO370001, 2011.

Proudman, J.: On the currents in the North Channel of the Irish Sea, Mon. Not. Roy. Astr. Soc., Geophys. Supp., 4, 387–403, 1936.

Proudman, J.: On tidal variation of temperature in the Irish Sea, Proc. Roy. Soc., 4, 373–386, doi:10.1111/j.1365-246X.1938.tb01762.x, 1938.

Proudman, J.: On the salinity of the surface waters of the Irish Sea, Philos. T. R. Soc. Lond., A239, 579–592, 1946.

Proudman, J.: Dynamical Oceanography, Methuen & Co, London, 1953.

Proudman, J. and Doodson, A. T.: Time-relations in meteorological effects on the sea, Proc. Roy. Math. Soc., S2–24, 140–149, 1926.

Proudman, J., Lewis, H. M., and Dennis, A. L.: On the Temperature of the Surface Waters of the Irish Sea, Philos. T. R. Soc. A, 236, 261–302, doi:10.1098/rsta.1937.0003, 1937.

Pugh, D. T.: Tidal amphidrome movement and energy dissipation in the Irish Sea, Geophys. J. Roy. Astr. S., 67, 515–527, 1981.

Pugh, D. T.: Tides, surges and mean sea-level: a handbook for engineers and scientists, Wiley, Chichester, UK, 1987.

Rasmussen, S. O., Anderson, K. K., Svensson, A. M., Steffensen, J. P., Vinther, B. M., Clausen, H. B., Siggaard-Andersen, M.-L., Johnsen, S. J., Larsen, L. B., Dahl-Jensen, D., Bigler, M., Röthlisberger, R., Fischer, H., Goto-Azuma, K., Hansson, M. E., Ruth, U.: A new Greenland ice core chronology for the last glacial termination. J. Geophys. Res., 111, D06102, doi:10.1029/2005JD006079, 2006.

Roemmich, D., Gould, W. J., and Gilson, J.: 135 years of global ocean warming between the Challenger expedition and the Argo Programme, Nature Climate Change, 2, 425–428, doi:10.1038/nclimate1461, 2012.

Rohde, R., Muller, R. A., Jacobsen, R., Muller, E., Perlmutter, S., Rosenfeld, A., Wurtele, J., Groom, D., and Wickham, C.: A New Estimate of the Average Earth Surface Land Temperature Spanning 1753 to 2011, Geoinfor Geostat: An Overview, 1, 1, 7 pp., doi:10.4172/2327-4581.1000101, 2013.

Rooth, C.: Hydrology and ocean circulation, Prog. Oceanogr., 11, 131–149, doi:10.1016/0079-6611(82)90006-4, 1982.

Rudels, B.: Arctic Ocean circulation and variability – advection and external forcing encounter constraints and local processes, Ocean Sci., 8, 261–286, doi:10.5194/os-8-261-2012, 2012.

Screen, J. A. and Simmonds, I.: Exploring links between Arctic implication and mid-latitude weather, Geophys. Res. Lett., 40, 1–6, doi:10.1002/grl.50174, 2013.

Sharples, J., Ross, O. N., Scott, B. E., Greenstreet, S. P. R., and Fraser, H.: Inter-annual variability in the timing of stratification and the spring bloom in the North-western North Sea, Cont. Shelf Res., 26, 733–751, doi:10.1016/j.csr.2006.01.011, 2006.

Simmonds, I. and Rudeva, I.: The great Arctic cyclone of August 2012, Geophys. Res. Lett., 39, L23709, doi:10.1029/2012GL054259, 2012.

Simpson, J. H.: Density stratification and microstructure in the western Irish Sea, Deep-Sea Res., 18, 309–319, 1971.

Simpson, J. H. and Hunter, J. R.: Fronts in the Irish Sea, Nature, 250, 404–406, doi:10.1038/250404a0, 1974.
Simpson, J. H., Brown, J., Matthews, J., and Allen, G.: Tidal straining, density currents, and stirring in the control of estuarine stratification, Estuaries, 13, 125–132, 1990.
Sirevaag, A., de la Rosa, S., Fer, I., Nicolaus, M., Tjernström, M., and McPhee, M. G.: Mixing, heat fluxes and heat content evolution of the Arctic Ocean mixed layer, Ocean Sci., 7, 335–349, doi:10.5194/os-7-335-2011, 2011.
Smith, S. D.: Coefficients for sea surface wind stress, heat flux, and wind profiles as a function of wind speed and temperature, J. Geophys. Res.-Oceans, 93, 15467–15472, doi:10.1029/JC093iC12p15467, 1988.
Solanki, S. K.: Sunspots: an overview, Astron. Astrophys. Rev., 11, 153–286, doi:10.1007/s00159-003-0018-4, 2003.
Soloviev, A., and Lukas, R.: The near-surface layer of the ocean; structure, dynamics and applications, Springer, 2006.
Stigebrandt, A.: The North Pacific: a global-scale estuary, J. Phys. Oceanogr., 14, 464–470, doi:10.1175/1520-0485(1984)014<0464:TNPAGS>2.0.CO;2, 1984.
Straneo, F., Heimbach, P., Sergienko, O., Hamilton, G., Catania, G., Griffies, S., Hallberg, R., Jenkins, A., Joughin., I., Motyka, R., Pfeffer, W. T., Price, S. F., Rignot, E., Scambos, T., Truffer, M., and Vieli, A.: Challenges to Understanding the dynamic response of Greenland's marine terminating glaciers to oceanic and atmospheric forcing, B. Am. Meteorol. Soc., 94, 1131–1144, doi:10.1175/BAMS-D-12-00100.1, 2013.
Stroeve, J. C., Kattsov, V., Barrett, A., Serreze, M., Pavlova, T., Holland, M., and Meier, W. N.: Trends in Arctic sea ice extent from CMIP5, SMIP3 and observations, Geophys. Res. Lett., 39, L16502, doi:10.1029/2012GL052676, 2012.
Sündermann, J. and Pohlmann, T.: A brief analysis of North Sea physics, Oceanologia, 53, 663–689, doi:10.5697/oc.53-3.663, 2011.
Swanson, K. L. and Tsonis, A. A: Has the climate recently shifted?, Geophys. Res. Lett., 36, L06711, doi:10.1029/2008GL037022, 2009.
Taylor, G. I.: Effect of variation in density on the stability of superposed streams of fluid, P. R. Soc. London, 132, 499–523, doi:10.109/rspa.1931.0015, 1931.
Toggweiler, J. R. and Russell, J.: Ocean circulation in a warming climate, Nature, 451, 296–8, doi:10.1038/nature06590, 2008.

Turney, C. S. M. and Brown, H.: Catastrophic early Holocene sea level rise, human migration and the Neolithic transition in Europe, Quaternary Sci. Rev., 26, 2036–2041, doi:10.1016/j.quascirev.2007.07.003, 2007.
Turner, J. S.: Stratification and circulation produced by heating and evaporation on a shelf, J. Mar. Res., 56, 885–904, doi:10.1357/002224098321667404, 1998.
Van Sebille, E., England, M. H., and Froyland, G.: Origin, dynamics and evolution of ocean garbage patches from observed surface drifters, Environ. Res. Lett., 7, 044040, doi:10.1088/1748-9326/7/4/044040, 2012.
Verspecht, F., Simpson, J. H., and Rippeth, T. P.: Semi-diurnal tidal ellipse variability in a region of freshwater influence, Geophys. Res. Lett., 37, L18602, doi:10.1029/2010GL044470, 2010.
Visser, M., Batten, S., Becker, G., Bot, P., Colijn, F., Damm, P., Danielssen, D., Van Den Eynde, D., Føyn, L., Frohse, A., Grueneveld, G., Laane, R., Van Raaphorst, W., Radach, G., Schultz, H., and Sündermann, J.: Time series analysis of monthly mean data of temperature, salinity, nutrients, suspended matter, phyto- and zoo-plankton at eight locations on the Northwest European Shelf, Deutsche hydrographische Zeitschrift, German Journal of Hydrography, 48, 299–323, doi:10.1007/BF02799376, 1996.
Waldbusser, G. G., Brunner, E. L., Haley, B. A., Hales, B., Langdon, C. J., and Prahl, F. G.: A developmental and energetic basis linking larval oyster shell formation to acidification sensitivity, Geophys. Res. Lett., 40, 2171–2176, doi:10.1002/grl.50449, 2013.
Walsh, J. E.: Melting ice: What is happening to Arctic sea ice, and what does it mean for us?, Oceanography, 26, 171–181, doi:10.5670/oceanog.2013.19, 2013.
Wanner, H., Brönnimann, S., Casty, C., Gyalistras, D., Luterbacher, J., Schmutz, C., Stephenson, D. B., and Xoplaki, E.: North Atlantic Oscillation – concepts and studies, Surv. Geophys., 22, 321–381, 2001.
Wendler, G. and Shulski, M.: A century of climate change for Fairbanks, Alaska, Arctic, 62, 295–300, 2009.
Wijesekera, H. W., Rudnick, D. L., Paulson, C. A., Pierce, S. D., Pegau, W. S., Mickett, J., and Gregg, M. C.: Upper ocean heat and freshwater budgets in the eastern Pacific warm pool, J. Geophys. Res.-Oceans, 110, C08004, doi:10.1029/2004JC002511, 2005.
Wijffels, S. E., Schmitt, R. W., Bryden, H. L., and Stigebrandt, A.: Transport of freshwater by the oceans, J. Phys. Oceanogr., 22, 155–162, doi:10.1175/1520-0485(1992)022<0155:TOFBTO>2.0.CO;2, 1992.

Williamson, D. I.: Planktonic evidence for irregular flow through the Irish Sea and North Channel in the autumn of 1954, J. Mar. Biol. Assoc. UK, 35, 461–466, 1956.
Williamson, D. I.: Hybridization in the evolution of animal form and life-cycle, Zoological Journal Linnaean Society, 148, 585–602, doi:10.111/j.1096-3642.2006.00236.x, 2006.
Williamson, D. I.: Caterpillars evolved from onychophorams by hybridogenesis, P. Natl. Acad. Sci. USA, 108, 19901–19905, doi:10.1073/pnas.0908357106, 2009.
Williamson, D. I.: Introduction to larval transfer, Cell Dev. Biol., 1, 1085, doi:10.4172/2168-9296.1000108, 2012.
Williamson, D. I. and Boerboom, N. G.: Experimental hybrids between ascidians and sea urchins, Cell Dev. Biol., 1, 2337, doi:10.4172/scientificreports.230, 2012.
Woodgate, R. A., Weingartner, T., and Lindsay, R.: The 2007 Bering Strait oceanic heat flux and anomalous Arctic sea-ice retreat, Geophys. Res. Lett., 37, L01602, doi:10.1029/2009GL041621, 2010.
Young, E. F. and Holt, J. T.: Prediction and analysis of long-term variability of temperature and salinity in the Irish Sea, J. Geophys. Res., 112, C01008, doi:10.1029/2005JC003386, 2007.
Yu, Y., Maykut, G. A., and Rothrock, D. A.: Changes in the thickness distribution of Arctic sea ice between 1958–1970 and 1993–1997, J. Geophys. Res., 109, C08004, doi:10.1029/2003JC001982, 2004.
Zhang, J. and Rothrock, D. A.: Modelling global sea ice with a thickness and enthalpy distribution model in generalized curvilinear coordinates, Mon. Weather Rev., 131, 681–697, 2003.

Table 1a. PEMBS 1904–2012 sea surface temperature °C changes and trends °C yr^{-1}.

Period	1904–2012	ΔT °C yr^{-1}	1904–1939	ΔT °C yr^{-1}	1940–86	ΔT °C yr^{-1}	1987–2012	ΔT °C yr^{-1}
Min	9.14	−0.94	9.14	−0.74	9.28	−0.94	10.07	−0.75
Y Min	1917	1962	1917	1915	1963	1962	1987	1996
Mean	10.46	0.01	10.24	0.02	10.37	−0.02	10.98	0.06
Std Dev	0.52	0.45	0.42	0.41	0.42	0.50	0.45	0.44
Max	11.66	1.25	10.88	0.95	11.54	1.25	11.66	0.79
Y Max	2007	1964	1933	1921	1959	1964	2007	1997

Table 1b. PEMBS 1904-2012 period trends and temperature changes.

Trend	Years	Linear	Log	Σ °C
1904–2012	109	0.0093	1.0009	1.01
1904–1939	36	0.018	1.0024	0.66
1940–1986	47	−0.0024	0.9998	−0.11
1987–2012	26	0.037	1.0034	0.96

Table 2a. Cypris Station 1954–2010 Sea surface temperature °C changes and trends °C yr^{-1}.

Period	1954–2010	1954–1986	1987–2010
Min	9.6	9.6	10.4
Y Min	1986	1986	1987
Mean	10.9	10.6	11.3
Std Dev	0.5	0.4	0.4
Max	11.8	11.8	11.8
Y Max	2003	1959	2003

Table 2b. Cypris Station 1954-2010 period trends and temperature changes.

Trend	Years	Linear	Log	Σ°C
1954–2010	57	0.017	1.002	1.0
1954–1986	33	−0.015	0.999	−0.5
1987–2010	24	0.033	1.003	0.80

Table 3a. Central England 1904–2011 land-air temperature °C changes and trends °C yr^{-1}.

Period	1904–2011	ΔT °C yr^{-1}	1904–1939	ΔT °C yr^{-1}	1940–86	ΔT °C yr^{-1}	1987–2011	ΔT °C yr^{-1}
Min	8.5	−1.8	8.5	−1.8	8.5	−1.4	8.8	−1.3
Y Min	1963	1922	1919	1922	1963	1962	2010	1996
Mean	9.6	0.0	9.4	0.0	9.5	−0.0	10.1	0.1
Std Dev	0.6	0.6	0.5	0.7	0.5	0.6	0.6	0.7
Max	10.8	1.9	10.5	1.1	10.6	1.2	10.8	1.9
Y Max	2006	2011	1921	1920	1949	1957	2006	2011

Table 3b. Central England 1904-2011 land-air period trends and temperature changes.

Trend CET	Years	Linear	Log	Σ °C
1904–2011	108	0.0085	1.0009	0.92
1904–1939	36	0.0151	1.0016	0.54
1940–1986	47	−0.0036	0.9996	−0.17
1987–2011	25	0.0183	1.0018	0.46

Table 4. PEMBS sea surface daily mean temperatures °C for three extreme winters; 1916–1917, 1962–1963 and 2010–2011.

Dec–Apr	2010–11	1962–63	1916–17
Min	6.74	3.50	3.33
Date Min	19 Dec	8 Feb	27 Jan
Av	8.40	6.64	6.61
Std Dev	0.91	1.91	1.90
Max	11.42	10.70	10.56
Date Max	16 Nov	16 Nov	16 Nov

Table 5. PEMBS monthly mean, min, max temperatures °C and trends °C yr^{-1}.

1904–2012	Jan	Feb	Mar	Apr	May	Jun	Jul	Aug	Sep	Oct	Nov	Dec
Min	5.66	4.50	5.18	5.75	7.73	9.34	11.13	12.66	12.47	11.14	8.90	7.99
Y Min	1963	1963	1947	1917	1917	1956	1956	1986	1986	1919	1919	1917
Mean	8.16	7.23	7.10	7.85	9.32	11.39	13.18	14.11	13.80	12.71	11.08	9.54
Std Dev	0.71	0.79	0.74	0.70	0.66	0.65	0.64	0.60	0.60	0.64	0.71	0.67
Max	9.58	9.08	8.85	9.50	11.19	12.89	14.51	15.44	15.14	14.38	12.64	11.08
Y Max	1998	1998	1998	2007	2007	2003	1959	2003	2006	1959	1997	1997
Max–Min	1.4	1.9	1.8	1.6	1.9	1.5	1.3	1.3	1.3	1.7	1.6	1.5
Lin trend	0.007	0.006	0.010	0.010	0.010	0.010	0.010	0.010	0.009	0.010	0.012	0.007
Σ*T* °C	0.78	0.71	1.09	1.10	1.13	1.08	1.07	1.05	1.03	1.04	1.26	0.81
1904–1939	Jan	Feb	Mar	Apr	May	Jun	Jul	Aug	Sep	Oct	Nov	Dec
Min	6.32	5.19	5.34	5.75	7.73	10.27	11.73	12.94	12.61	11.14	8.90	7.99
Y Min	1918	1917	1917	1917	1917	1916	1919	1920	1912	1919	1919	1917
Mean	8.02	7.12	6.82	7.52	9.02	11.07	12.92	13.87	13.55	12.37	10.69	9.26
Std Dev	0.63	0.58	0.65	0.56	0.42	0.41	0.54	0.48	0.55	0.54	0.64	0.62
Max	9.23	8.28	7.93	8.41	9.85	11.78	14.10	14.81	14.70	13.48	11.71	10.70
Y Max	1932	1935	1938	1938	1921	1937	1905	1933	1933	1921	1938	1924
Lin trend	0.024	0.020	0.019	0.017	0.010	0.015	0.015	0.013	0.026	0.017	0.025	0.017
Σ*T* °C	0.86	0.73	0.69	0.63	0.36	0.55	0.53	0.49	0.94	0.62	0.92	0.62
1940–1986	Jan	Feb	Mar	Apr	May	Jun	Jul	Aug	Sep	Oct	Nov	Dec
Min	5.66	4.50	5.18	6.45	7.79	9.34	11.13	12.66	12.47	11.38	9.83	8.24
Y Min	1963	1963	1947	1986	1956	1956	1956	1986	1986	1952	1952	1952
Mean	8.01	7.04	6.99	7.79	9.22	11.35	13.06	13.94	13.70	12.72	11.06	9.57
Std Dev	0.68	0.89	0.73	0.69	0.64	0.64	0.60	0.50	0.50	0.56	0.60	0.65
Max	8.93	8.26	8.37	9.04	10.61	12.53	14.51	15.13	14.97	14.38	12.60	11.06
Y Max	1973	1961	1959	1959	1960	1960	1959	1959	1959	1959	1956	1956
Lin trend	0.000	−0.004	−0.000	−0.010	−0.002	−0.000	0.001	−0.001	−0.003	−0.004	−0.003	−0.002
Σ*T* °C	0.00	−0.17	−0.01	−0.45	−0.10	−0.01	0.03	−0.05	−0.13	−0.20	−0.16	−0.11
1987–2012	Jan	Feb	Mar	Apr	May	Jun	Jul	Aug	Sep	Oct	Nov	Dec
Min	7.15	5.95	6.43	7.38	8.78	10.54	13.00	13.78	13.25	11.90	10.42	8.31
Y Min	1987	1991	1987	1994	1996	1991	1996	1994	1994	1993	1993	2010
Mean	8.63	7.72	7.68	8.42	9.93	11.88	13.76	14.72	14.33	13.16	11.65	9.88
Std Dev	0.68	0.66	0.53	0.53	0.59	0.64	0.46	0.48	0.53	0.63	0.63	0.62
Max	9.58	9.08	8.85	9.50	11.19	12.89	14.42	15.44	15.14	14.18	12.64	11.08
Y Max	1998	1998	1998	2007	2007	2003	2006	2003	2006	2006	1997	1997
Lin trend	0.017	0.018	0.031	0.050	0.046	0.055	0.042	0.041	0.044	0.046	0.040	0.010
Σ*T* °C	0.43	0.48	0.81	1.30	1.19	1.42	1.10	1.06	1.15	1.19	1.05	0.27

Table 6. CET monthly mean temperatures °C and trends °C yr^{-1} 1659–2011.

1659–2011	Jan	Feb	Mar	Apr	May	Jun	Jul	Aug	Sep	Oct	Nov	Dec	*Y*	Δ*T* °C yr^{-1}
Min	−3.1	−1.9	1.0	4.7	8.5	11.5	13.4	12.9	10.5	5.3	2.3	−0.8	6.8	−2.4
Y min	1795	1947	1674	1701	1698	1675	1816	1912	1674	1740	1782	1890	1740	1740
Av	3.2	3.9	5.3	7.9	11.2	14.3	16.0	15.6	13.3	9.7	6.1	4.1	9.2	0.01
Std Dev	2.0	1.8	1.5	1.2	1.1	1.1	1.2	1.1	1.1	1.3	1.4	1.7	0.7	0.7
Max	7.5	7.9	9.2	11.8	15.1	18.2	19.7	19.2	16.8	13.3	10.1	8.1	10.8	2.5
Y Max	1916	1779	1957	2011	1833	1846	2006	1995	2006	2001	1994	1934	2006	1741
Max–Min	7.5	7.9	9.2	11.8	15.1	18.2	19.7	19.2	16.8	13.3	10.1	8.1	10.8	
Linear trend	0.005	0.003	0.004	0.003	0.001	0.000	0.001	0.001	0.002	0.004	0.004	0.003	0.003	Σ yr
Σ*T* °C	1.7	1.0	1.5	0.9	0.5	0.0	0.5	0.5	0.7	1.3	1.2	1.2	0.9	353

Table 7. Temperature, salinity and density for 8 yr means 1999–2006 and 1982–1989.

	T 99–06	S 99–06	ρ 99–06	T 1982–9	S 1982–9	ρ 1982–89
Min	7.1	33.7	25.2	6.3	33.8	25.3
Day Min	28 Feb	8 Nov	6 Sep	20 Feb	8 Feb	30 Aug
T °C @ Min	7.1	12.3	15.2	6.3	7.0	13.9
S ‰ @ Min	34.0	33.7	34.1	34.0	33.8	33.9
Density σ @ Min	26.6	25.4	25.2	26.6	26.4	25.3
Av	11.3	34.1	25.9	10.3	34.0	26.0
StDev	2.6	0.1	0.5	2.6	0.1	0.4
Max	15.2	34.4	26.6	14.2	34.2	26.7
Day Max	2 Sep	8 Jan	5 Mar	18 Aug	15 May	18 Feb
T °C @ Max	15.2	9.3	7.4	14.2	9.0	6.4
S ‰ @ Max	34.2	34.4	34.2	34.1	34.2	34.0
Density σ @ Max	25.2	26.5	26.6	25.4	26.4	26.7

Table 8a. Arctic sea ice volume in 10^3 km^3 for two 8 yr periods, 1979–86 and 2005–12. Data courtesy of PIOMAS, Zhang and Rothrock (2003). Arctic sea ice extent in 10^6 km^2 courtesy of Fetterer, F., Knowles, K., Meier, W., and Savoie, M. (2002), updated 2009. *Sea Ice Index*. Boulder, Colorado USA: National Snow and Ice Data Center, Digital media.

Volume 10^3 km^3	Min	Day	Mean	Max	Day	Max−Min
1979–86	14.9 ± 1.4	12 Sep	23.4 ± 1.2	31.1 ± 1.2	24 Apr	16.2 ± 0.9
2005–12	6.3 ± 2.2	16 Sep	15.4 ± 1.9	24.1 ± 1.6	15 Apr	17.8 ± 0.9

Table 8b. Arctic sea ice volume period trends.

Trend Volume 10^3 km^3 yr^{-1}	Min		Mean		Max	
8 yr	Linear	Log	Linear	Log	Linear	Log
1979–86	−0.088	0.995	−0.180	0.993	−0.237	0.973
2005–12	−0.862	0.863	−0.731	0.953	−0.565	0.977

Table 8c. Arctic sea ice area period maximum, minimum and differences.

Area 10^6 km^2	Min	Day	Mean	Max	Day	Max−Min
1979–86	7.0	8 Sep	12.2 ± 0.2	16.1	12 Mar	9.1
2005–12	4.7	7 Sep	10.7 ± 0.2	15.0	16 Mar	10.4

Table 8d. Arctic sea ice area period trends.

Trend Area 10^6 km^2 yr^{-1}	Min		Mean		Max	
8 yr	Linear	Log	Linear	Log	Linear	Log
1979–86	−0.060	0.991	−0.040	0.997	−0.043	0.997
2005–12	−0.225	0.951	−0.051	0.995	0.038	1.002

Table 8e. Arctic sea ice thickness period maximum and minimum.

Thickness Vol/Area m	Sep Min	Mean	Mar Max	Max−Min
1979–86	2.1	1.9	1.9	−0.2
2005–12	1.4	1.4	1.6	+0.2

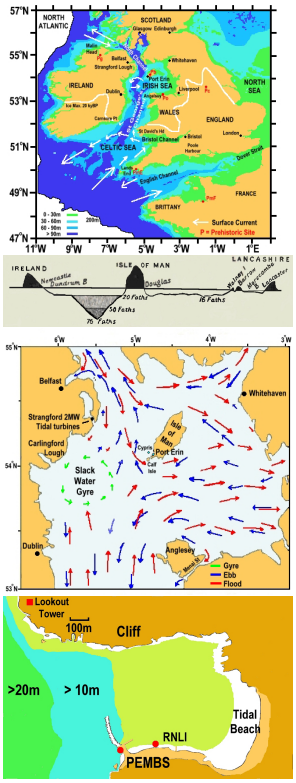

Fig. 1. (a) Irish Sea western fjord **(b)** Bathymetric cross section through Isle of Man fjord 76 fathoms, eastern Irish Sea 16 fathoms (Herdman, 1920) 1 fathom = 1.83 m **(c)** Irish Sea flood, ebb and gyre surface currents, **(d)** Inset Port Erin Bay.

115

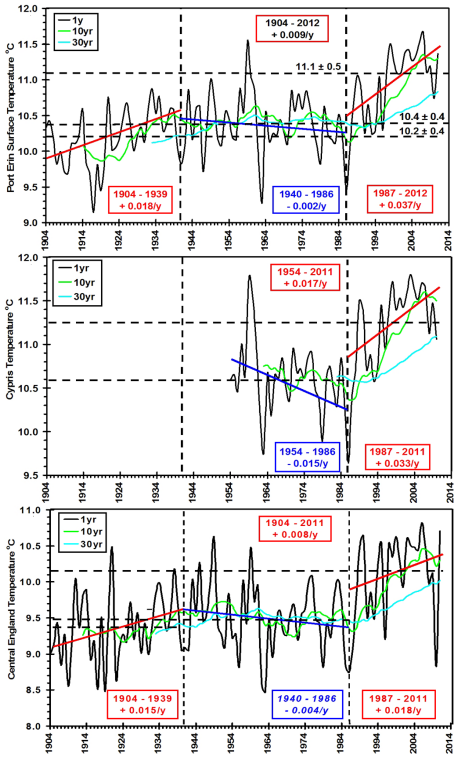

Fig. 2. Running means and trends for **(a)** PEMBS, Isle of Man SST 1904–2012. **(b)** Cypris station, Isle of Man SST 1954–2011 **(c)** CET land-air temperatures 1904–2011.

116

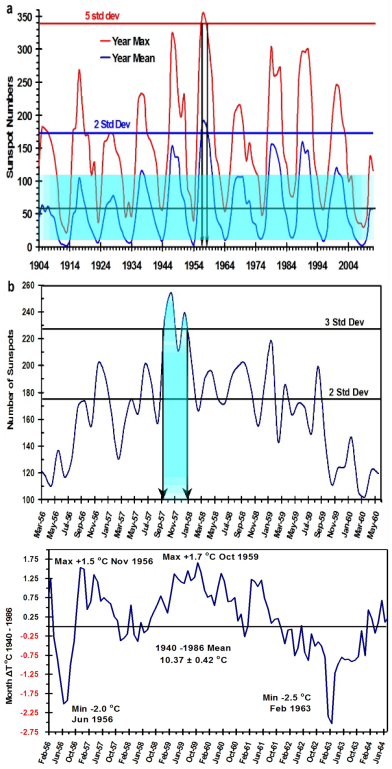

Fig. 3. Sunspot numbers **(a)** 1904–2012 arrows mark year maximum > 5 standard deviations above mean **(b)** March 1956–May 1960 arrows mark months > 3 standard deviations above long-term mean **(c)** Port Erin SST differences from monthly means 1940–1986.

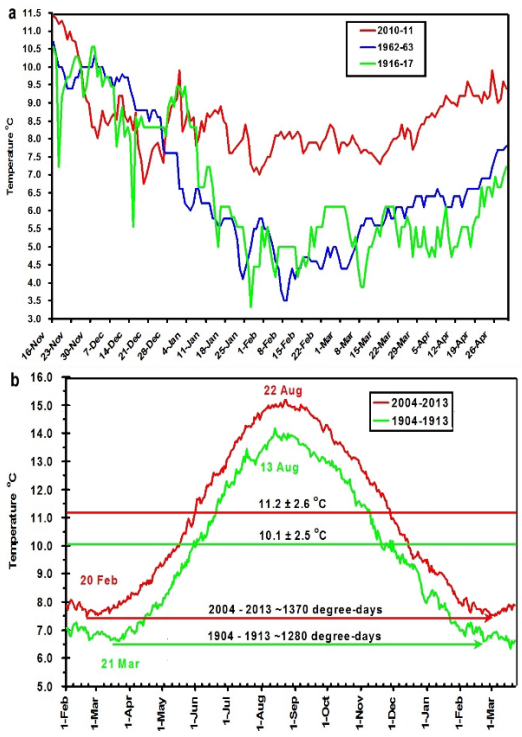

Fig. 4. (a) Daily Port Erin bay SST for winters December through April 1916–1917, 1962–1963 and 2010–2011 **(b)** Port Erin 10 yr mean annual heating cycles for 1904–1913, and 2004–2013 in degree-days with means, minimum and maximum dates.

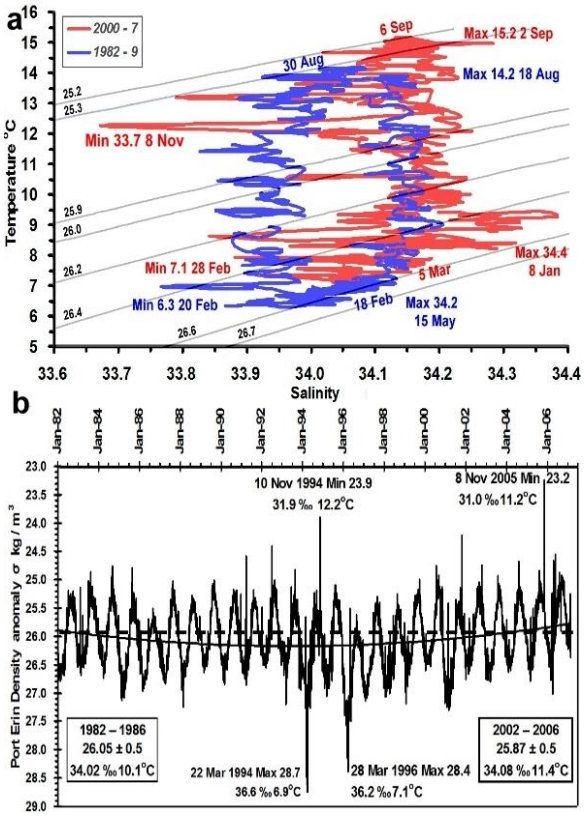

Fig. 5. (a) Daily mean seasonal TS 8 yr cycles 1982–1989 and 1999–2006 **(b)** Daily density 1982–2006 with second order polynomial trend.

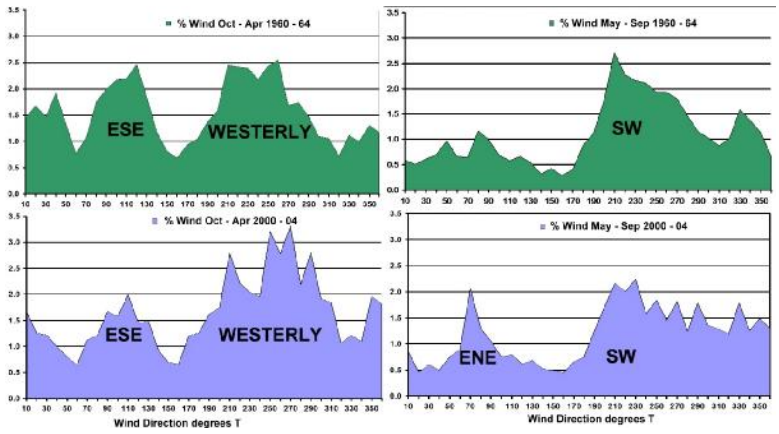

Fig. 6. Ronaldsway, Isle of Man airport, (54.09° N 4.63° W), wind direction for winter (October–April) and summer (May–September) for 5 yr periods 1960–1964 and 2000–2004.

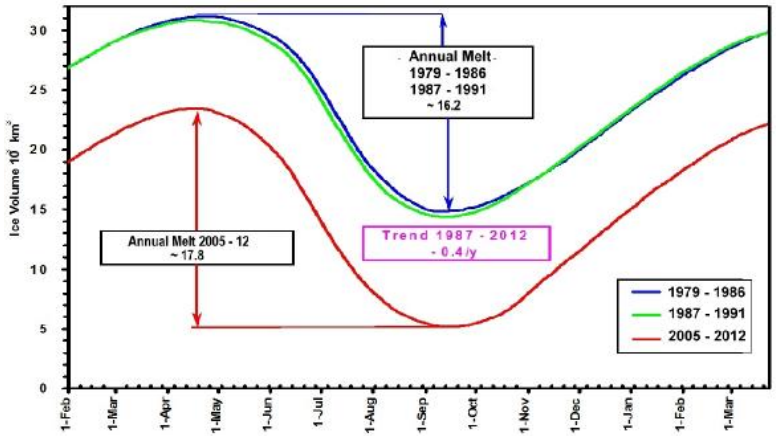

Fig. 7. Annual cycle of ice volume melt for 5 yr periods 1979–1986, 1987–1991 and 2005–2012. Data courtesy of Zhang and Rothrock, 2003) (http://psc.apl.washington.edu/wordpress/research/projects/arctic-sea-ice-volume-anomaly/data/).

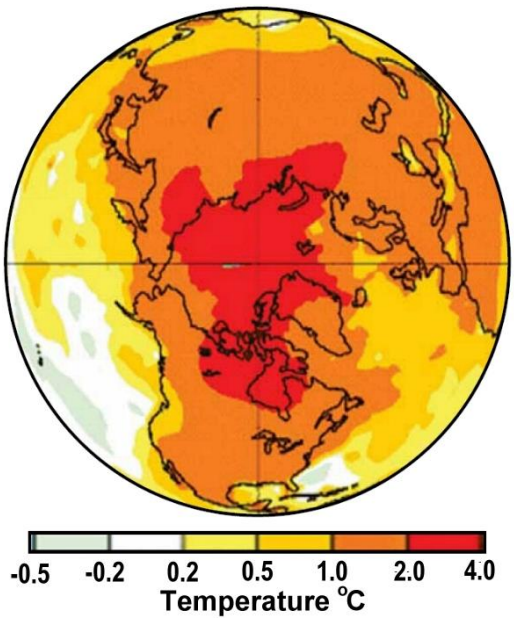

Fig. 8. NASA GISS temperature rise 1963–2012 showing polar amplification reprinted by permission Oceanography Society and J. E. Walsh from Walsh (2013).